Los Alamos National Laboratory is operated by the University of California for the United States Department of Energy under contract W-7405-ENG-36.

A Model for Computing Late Detonations Initiated in Propellants by Impact (XDT Reactions)

Los Alamos
Los Alamos National Laboratory
Los Alamos, New Mexico 87545

This work was supported by the US Navy Strategic Systems Project Office.

Prepared by Maelo Chapin, Group M-4

LA-10270-MS

UC-45
Issued: November 1984

A Model for Computing Late Detonations Initiated in Propellants by Impact (XDT Reactions)

Robert R. Karpp*

*Current affiliation: Aerojet Ordnance Co., 2521 Michelle Drive, Tustin, CA 92680.

Los Alamos National Laboratory
Los Alamos, New Mexico 87545

A MODEL FOR COMPUTING LATE DETONATIONS INITIATED IN PROPELLANTS BY IMPACT (XDT REACTIONS)

by

Robert R. Karpp

ABSTRACT

A computational model that produces simulations of impact-initiated late detonations in rocket motor propellants has been constructed and incorporated into hydrodynamic computer codes. For high-speed impacts between cylindrical propellant projectiles and steel plates, the model correctly predicts the shock-to-detonation transition. For low-speed impacts, the model correctly predicts the absence of detonation. At intermediate speeds where late detonations occur with reasonable probability, the model predicts the eventual development of detonation. The model is based upon the hypothesis that late detonations occur when the propellant from the front portion of the projectile that is damaged during the early stage of impact is impinged upon by the rear portion of the projectile, which is still moving toward the target with significant speed. This recompression of damaged, sensitive propellant appears to be the primary initiating mechanism of the XDT reaction. This conclusion is substantiated by agreement between test data and calculations based upon that hypothesis.

I. INTRODUCTION

This report summarizes work accomplished under the reimbursable project R377 sponsored by the Navy Strategic Systems Project Office for fiscal years 1980, 1981, and 1982. This work was in support of and coordinated with investigations by Hercules-Thiokol (Joint Venture) of the detonation hazards of the Trident-I (C-4) rocket motor.

The purpose of this project was to computationally model "late detonations" that occur in propellant impact tests of some rocket motor propellants and to identify the significant mechanisms that cause the detonations. Investigators

at Hercules, Inc., discovered that cylindrical projectiles of propellant fired at steel target plates can eventually detonate at impact velocities well below those required for the usual shock-to-detonation transition. This new late detonation phenomenon is now widely known as XDT and is important in the assessment of propellant hazards.

In order to reduce the parameters involved in the study, we have concentrated our attention on one particular propellant designated as VRP. Several finite-difference, hydrodynamic codes were used in this study; however, the majority of the calculations were performed with the HELP[1] and the SALE[2] codes.

The next section of this report indicates the experimental work that had been conducted to understand the nature of late detonations in propellant impacts. The equation of state used to represent the reacted and unreacted propellant in the code calculations is presented in Section III. The next section shows computer simulations of inert impacts. This section is important because it delineates the dynamics of impact and reveals the development of the recompression phenomenon, which is thought to be the significant mechanism that triggers late detonations. Section V describes the basic version of the reaction rate formula (DAGMAR), which is used in the computational model. A demonstration that DAGMAR adequately predicts the shock-to-detonation transition in VRP propellant is given in Section VI. The next section describes the modifications made to DAGMAR and to the computational scheme in order to simulate the XDT phenomenon. Two examples of the simulation of XDT, one for the small shotgun projectile and one for the large, 152-mm-diam, 105-mm-long projectile, are given in Section VIII. These simulations are in good agreement with radiographic observations of XDT. Also, the calculated relationship between threshold velocity and projectile diameter is shown to be in good agreement with the experimentally observed relationship. The results of this work are summarized in Section IX. The main result is that a computational model has been constructed that reproduces the experimentally observed features of the XDT reaction.

II. EXPERIMENTAL OBSERVATIONS

The experiment considered during the modeling study consists of a smoothbore gun firing a cylindrical projectile of propellant against a steel target plate. These tests were conducted by Joint Venture at the Hercules, Inc., plant in Magna, Utah, with 18- and 25-mm-diam guns and at Hercules Allegheny Ballistic

Laboratory, Rocket Center, West Virginia, with a 70-mm-diam gun. Slightly different impact tests were performed at the Lawrence Livermore National Laboratory with a 155-mm-diam gun.

A schematic of the 18-mm gun test (the shotgun test) is shown in Fig. 1, taken from Ref. 3. The primary diagnostic used with this test is flash radiography of the projectile during impact. From the radiographs, the occurrence of a detonation, as well as the approximate time of detonation, can be determined. The direct shock-to-detonation transition (SDT) can easily be identified by its promptness. An example of radiographs showing SDT is given in Fig. 2, taken from Ref. 4. At impact velocities that are much lower than the threshold velocity for SDT, a low-order reaction may occur that is not a detonation. This reaction is illustrated in Fig. 3. However, at impact velocities that are intermediate to or overlapping with the above two cases, a second type of impact-initiated detonation may occur. This second transition to detonation occurs after considerable deformation and breakup have taken place in the propellant projectile. Because of its unknown origin, this late detonation has been termed XDT. This reaction is illustrated in the radiographs of Fig. 4. The purpose of this work is to model the XDT process.

Pressure gauges mounted a few feet from the impact point have been used in some tests to measure the blast pressure resulting from the reaction. The greatest blast pressure is generated by the XDT reaction. Somewhat lower pressures are developed by the SDT reaction, and the lowest pressures result from the low-order reactions.

In some tests, Manganin pressure gauges were imbedded in the steel target plate just under the point of impact. These records give an indication of the pressure history near the point of impact.

The results of many propellant impact tests are summarized in Table I, adapted from Ref. 5. The minimum impact velocities required to initiate either the SDT or the XDT reaction are listed along with the time to detonation and probability of detonation for the XDT reaction.

III. EQUATION OF STATE OF PROPELLANTS

The propellant material was treated as an inviscid, compressible fluid with no resistance to shear deformation. Although the propellant does have some strength, calculations of impacts based upon the fluid model are in excellent agreement with radiographic data.[6]

The equation of state used to describe the propellant is the HOM equation of state described in Ref. 7. In this treatment, separate equations are used to describe each phase of the material, the unreacted solid and the completely reacted gas. The pressure in the unreacted solid propellant is determined from a Mie-Grüneisen form, with a constant Grüneisen coefficient, referred to the principal Hugoniot. For the completely reacted gaseous phase, a Mie-Grüneisen form, with a variable Grüneisen coefficient, referred to the C-J isentrope is used. The Hugoniot for the unreacted propellant is determined experimentally, but the C-J isentrope for the completely reacted propellant is determined from thermochemical calculations. Temperature is also obtained from the HOM equation of state by using the assumption of constant specific heats for both phases.

In the computation of a reaction, the reaction variable λ, mass fraction of reacted material, is used to measure the extent of reaction. In the computational scheme, a calculational zone with the value $\lambda = 0.25$ implies that 25% of the material has been completely reacted and 75% is unreacted. For zones containing both reacted and unreacted material, the state is usually determined by assuming pressure and temperature equilibrium between the two phases. Many of the calculations performed in this work used the above pressure and temperature equilibrium rule. However, some of the calculations were based upon a simpler mixing rule that "blends" the pressure P and temperature T together by

$$P = (1 - \lambda)P_S + \lambda P_G \quad ,$$

$$T = (1 - \lambda)T_S + \lambda T_G \quad ,$$

where the subscript S stands for solid and G stands for reacted gas. The results obtained with either mixing rule are qualitatively similar and, through proper calibration, could probably produce reasonable quantitative agreement. The specific equations and values for the coefficients used in the HOM equation of state are given in Appendix A.

IV. SIMULATION OF INERT IMPACT

In this work, the first hydrocode simulations of impact were performed with the propellant material treated as inert. The calculations were based on the HOM equation of state with the reaction variable λ held equal to zero; therefore, only the unreacted solid portion of the equation of state was used. Figure 5 shows pressure contours at several times taken from a HELP code calculation of a 700-m/s impact of a shotgun projectile (18 mm diam by 19 mm long) against a rigid target. This impact velocity is within the range of interest

for the XDT reaction and produces an initial shock pressure of 42 kbar. The propellant is modeled as an inviscid, compressible fluid with no cohesive strength (minimum pressure of zero) or shear strength.

At 2.5 μs after impact (upper left frame of Fig. 5), the shock has decayed to 33 kbar due to the interaction with the cylindrical rarefaction wave that initiates from the lateral free surface of the propellant cylinder. At 5 μs after impact, the shock wave just reaches the end of the propellant, and the shock strength has decreased to about 10 kbar. The lateral rarefaction wave has reflected from the axis of symmetry and caused a region of low density. The effects of this cylindrical rarefaction wave are significant because of the convergent geometry. Also, a secondary region of high pressure has started to form near the impact face at a radius of 1 cm. This region consists of propellant material that has been rarefied by the lateral rarefaction wave and then recompressed by material above it, which is still moving toward the impact plane. The remaining frames of Fig. 5 show the development of this recompaction or recompression region. This region eventually covers the entire lower half of the projectile, and the maximum pressure developed in this region is in excess of 6 kbar.

Figure 6 shows a three-dimensional plot of the pressure distribution over the impacting cylinder. As in the previous figure, the development of the recompaction region is clearly shown. It is important to note that the recompaction region forms at a very early time (less than 5 μs for the shotgun test) and persists throughout most of the motion (greater than 15 μs for the shotgun test). Figure 7 shows pressure histories at various points on the axis of symmetry for this calculation of a shotgun projectile impact. The recompression pulse initiated at about 10 μs after impact is clearly evident.

Green et al.[8] have indicated that the rarefaction/recompaction process probably initiates the XDT reaction. This statement is plausible because the rarefied material is in a highly damaged state and, therefore, may be very sensitive to rapid pressure loading. In this work, we assume that the recompaction pressure pulse is the stimulus for the XDT reaction.

V. REACTION RATE EQUATION

In this work, the reaction is modeled by allowing the reactants to transform directly to final products. The state of the reaction is then completely specified by the mass fraction of the products, λ. The reaction is

described by a reaction rate equation that specifies the evolution of λ. In this study, two reaction rate equations have been used to model propellants reacting during impact, FOREST FIRE[7,9] and DAGMAR[10]; however, we have made more use of the DAGMAR equation, and, therefore, its formulation is indicated here.

A form of the DAGMAR (direct analysis generated modified Arrhenius rate) decomposition rate model has been incorporated into our hydrocodes. DAGMAR is currently formulated as

$$\dot{\lambda}/(1 - \lambda) = Z_0 P_S^n G \, e^{-T^*/T} \quad ,$$

where the induction time factor, G, is

$$G(t) = e^{-C_1/I(t)} \quad ,$$

with

$$I(t) = \int_0^t \left(p(\tau) - C_2\right)^2 d\tau. \tag{1}$$

In these expressions, P_S is the pressure of the first shock that processes the material particle, T and p are the instantaneous absolute temperature and pressure, and Z_0, n, C_1, C_2, and T* are constants for a particular reactive material. The values of the constants used to describe VRP are given in Appendix B. In addition, the reaction rate, $\dot{\lambda}$, is maintained at zero until the pressure exceeds a threshold value, P_I. These equations are to be applied along a particle path; that is, $\dot{\lambda}$ is a material time derivative, and the integral, I, is summed along a particle path. Thus, in the DAGMAR model there are three progress variables, λ, P_S, and I. The evolutionary equations for these variables are

$$\dot{\lambda} = (1 - \lambda) Z_0 P_S^n G \, e^{-T^*/T} = R_1 \quad , \tag{2}$$

$$\dot{P}_S = 0 = R_2 \quad , \tag{3}$$

$$\dot{I} = (p - C_2)^2 = R_3 \quad . \tag{4}$$

These equations can be summarized as

$$\dot{\lambda}_i = R_i \quad (i = 1,2,3) \quad , \tag{5}$$

where $\lambda_1 = \lambda$, $\lambda_2 = P_s$, and $\lambda_3 = I$.

With a Eulerian code, the λ_i must evolve according to both a local rate of change and a rate of change due to transport. With a Lagrangian code, the change due to transport is of course zero. Equation (5) can be put in Eulerian form by combining each equation individually with the continuity equation. The result of this combination is

$$\frac{\partial(\rho\lambda_i)}{\partial t} + \frac{\partial(\rho v_r \lambda_i)}{\partial r} + \frac{\rho v_r \lambda_i}{r} + \frac{\partial(\rho v_z \lambda_i)}{\partial Z} = \rho R_i \quad , \tag{6}$$

where ρ is the mass density, v_r and v_z are the velocity components, and r and z are cylindrical coordinates. For plane flow the third term in Eq. (6) is not present, and r and z are replaced by x and y. Equation (6) is now in the same form as the conservation equations that are numerically solved by Eulerian codes. Therefore, this equation can be differenced in exactly the same manner. To be consistent with the HELP algorithm, the contribution to the time derivative of the source term (term on the right side) in Eq. (6) is first computed. Then all variables are updated. Next, the contribution to the time derivative is computed from the transport terms in Eq. (6), and all variables are again updated. This calculational procedure has been programmed into the HELP code. In program SALE, Eq. (5) is represented by first order forward difference equations that are advanced at the end of the Lagrangian phase, and no provision has been made for convection of the λ_i. Therefore, in this study, SALE has been used in its Lagrangian form only.

The DAGMAR model is quite sensitive to the shock pressure, P_s. For codes that use shock smearing techniques to treat shock waves, the shock pressure is not a well-defined quantity. For one-dimensional Lagrangian calculations with the PAD code,[11] a rather elaborate technique is used to calculate the shock pressure. For the two-dimensional implementation of DAGMAR, this elaborate technique may be too time consuming; therefore, we have tried to use a simpler method. Currently the method in use is based upon the fact that in numerically calculated shocks the artificial viscosity increases to a maximum and then decreases. The point of maximum artificial viscosity is a good indication of

the shock position. The pressure at that point is approximately one-half the shock pressure. To determine the shock pressure, the code monitors the value of artificial viscosity in each zone. When the artificial viscosity passes the maximum value and decreases to just less than 10% of that maximum value, the pressure on that cycle is taken as the shock pressure for that particular zone. The 10% value is of course arbitrary, and we have tried values from 10% to 25%. For a one-dimensional test problem, all these values appear to give adequate results.

VI. SIMULATION OF THE SHOCK-TO-DETONATION TRANSITION (SDT)

Much detailed information concerning the shock-initiated buildup to detonation of energetic materials must be acquired to determine all constants in the DAGMAR model. For VRP at normal density, we have only the one-dimensional wedge test data (input shock pressure vs run distance to detonation) to determine the DAGMAR constants. However, a set of constants that is consistent with the shock initiation data can be assumed; see Appendix B for these values. The data points (from Ref. 12) and the curve in the upper portion of Fig. 8 show a comparison between shock initiation data for VRP at normal density and one-dimensional calculations based upon the DAGMAR model. The calculated results are quite representative of the data.

Figure 9 shows some results of computer simulations of the shotgun test based upon the above calculational model. The upper two frames of Fig. 9 show examples of the SDT process with impact speeds of 911 and 1143 m/s. These speeds are well into the SDT range. The lower two frames show an impact calculation at just below the threshold velocity for SDT in VRP. The calculation correctly indicates that buildup to detonation does not occur. However, when the calculated results are compared with radiographs, the calculation appears to overestimate the amount of reacted material. Figure 10 shows the pressure history near the center of impact from a calculation with the standard DAGMAR model (curve D) and from a calculation with the propellant treated as inert (curve I). The two calculated pressure histories are qualitatively different because the inert calculation clearly indicates the recompression pressure pulse, while the DAGMAR calculation does not. Manganin pressure gauges imbedded below the impact surface indicate a recompression pulse similar to the calculated result of curve I; see Ref. 5 for data. We conclude that the DAGMAR model is predicting too much reaction as a result of the initial shock, and the quenching effect of the

lateral rarefaction waves is not being adequately modeled. However, a minor modification has been made to DAGMAR in order to adequately treat the quenching effect. This modification is described in the next section.

VII. MODELING THE XDT REACTION

In this work, we base the initiation mechanism of XDT upon the recompression pressure pulse that occurs in the freshly damaged propellant material. As indicated in the previous section, the current calibration of the DAGMAR model does not predict recompression because the model produces excessive reaction. However, we can allow the DAGMAR model to better include the rapid quenching effect of the lateral rarefaction wave by allowing P_s to decrease if the current pressure falls below the first shock pressure. Therefore, we introduce the minor modification of DAGMAR that

$$P_s = P_1 \text{ if } P \geq P_1, \text{ and}$$
$$P_s = P \text{ if } P < P_1 \quad ,$$

where P is the current pressure, P_1 is the first shock pressure, and P_s is the quantity in the DAGMAR formula. Calculations with this change in DAGMAR agree more closely with the experimental data from radiographs and pressure gauges.

Because the triggering effect of recompression occurs in material that is highly damaged, we need to describe the shock sensitivity of damaged propellant in the reaction model. The data points in the lower portion of Fig. 8 (from Refs. 13 and 14) show the shock initiation sensitivity of propellants that are granulated and repacked to a low density (72 and 50% of the intact density). Figure 8 indicates the large difference in sensitivity between intact and damaged propellants; damaged propellants are much more sensitive. We therefore assume that the damaged material is described by a new set of constants in the DAGMAR model. These new constants are given in Appendix B. Another change in the DAGMAR model for damaged propellant is that the current pressure is used in place of P_s. Because we do not have data on the shock sensitivity of granulated propellants at various densities, we assume that the change in sensitivity is discontinuous. If the material maintains a density of greater than 95% of the intact density, we assume the material is undamaged and use DAGMAR constants appropriate to undamaged material. If the material density drops below 95%, and if the material is relatively unreacted ($\lambda < 5\%$), we use DAGMAR constants appropriate to damaged propellant.

The lower curve in Fig. 8 was obtained from one-dimensional shock initiation calculations using the modified DAGMAR model with the constants given in Appendix B. The curve is in reasonable agreement with the data. At this point in the modeling process, the two curves in Fig. 8 represent the shock initiation sensitivity of the intact and damaged propellant.

It should be mentioned that, when use is made of the modified DAGMAR model, the induction time factor G(t) starts increasing in value, at a material element, when the first shock wave passes over that element. For typical impact speeds, the value of G(t) increases as a result of the action of the first pressure pulse from zero to a value usually greater than 0.7. Therefore, the second pressure pulse, the recompression pulse, is applied to a material that is sensitized because its value of G(t) is already near unity. Thus, the calculational procedure treats freshly damaged propellant as more sensitive than previously damaged propellant. This treatment is plausible because freshly damaged propellant may be burning.

VIII. SIMULATION OF XDT

Figures 11-16 show two different examples of computer simulations of the XDT reaction. These two calculations pertain to the two extreme cases that were experimentally studied, the small shotgun projectile and the large 152-mm-diam, 105-mm-long projectile. The calculations are based upon the modified DAGMAR model described in the previous section.

Figures 11, 12, and 13 show results from calculations of the shotgun test at an impact velocity of 700 m/s. Figure 11 shows the velocity field at four different instants of time. At 14 μs after impact, the reaction appears to be just starting in the computational zone nearest the target at a radial position of about 0.7 cm. At 16 μs the reaction is clearly established, and at 18 μs the reaction is complete. Figures 12 and 13 show the pressure contours and the degree of reaction contours for the same sequence of times.

Figures 14, 15, and 16 show results from the calculation of a 300-m/s impact of a 152-mm-diam, 105-mm-long VRP projectile against a rigid target. Figure 14 shows the velocity field at four different instants of time. The XDT reaction occurs between 175 and 210 μs. Figures 15 and 16 show the pressure and degree of reaction contours for the same sequence of times. From Fig. 16, it appears that the reaction may be just starting at 175 μs in the computational zone nearest the impact face at a radius of 6 cm.

In the above two calculations, the apparent initiation point for the XDT reaction was not on the axis, but at a substantial radius. At high impact velocities within the XDT range, the initiation point, according to this model, will be at a substantial distance from the axis. As the impact velocity is lowered within the XDT range, the initiation point will move closer to the axis. This effect is due to the nature of the recompression phenomenon. The recompression first develops near the periphery of the projectile. The region of compression then spreads toward the axis, and, as it spreads, it grows in strength. Figures 5 and 6 illustrate the recompression buildup and show that the maximum pressure eventually occurs on the axis. At high impact velocities within the XDT range, the early stage of recompression reaches high enough pressures for long enough times to initiate the XDT reaction in the sensitive, freshly damaged propellant. At low impact velocities within the XDT range, the early stage of recompression does not produce high enough pressures for long enough times to initiate the reaction. However, as recompression develops and pressures increase, the conditions for initiation may be met during the later stages of recompression near the axis of symmetry. The effect is illustrated in Fig. 17 where degree of reaction contours calculated for a low impact velocity of 550 m/s in the shotgun test are shown. The point of initiation is near the axis of symmetry. Figure 17 should be compared with Fig. 13 to see the difference in initiation between high and low impact velocities. Similar situations appear to exist for various sized projectiles all having the length-to-diameter ratio (L/D) of the shotgun test (L/D = 1.1). However, in the large diameter test (152-mm diam, 105-mm-long, L/D = 0.7), the projectile must initiate at a point (or ring) fairly far from the axis because the later stages of recompression are not realized as a result of early pressure release from the rear free surface.

The XDT threshold velocity (minimum impact velocity required to initiate the XDT reaction) is plotted as a function of projectile diameter in Fig. 18 from values given in Table I. The experiments were conducted with specimens having L/D = 1.1 but with three different diameters: the shotgun-size projectile, the 25-mm-diam projectile, and the 70-mm-diam projectile. One data point for the 152-mm-diam projectile with L/D = 0.7 is also plotted. A plot of the calculated threshold velocity obtained from two-dimensional hydrocode calculations is also shown (solid curve) for projectiles with L/D = 1.1. The calculated threshold velocity for the 152-mm-diam projectile (L/D = 0.7) is also

shown (dotted curve). The calculated relationship between threshold velocity and projectile diameter is in good agreement with the relationship observed experimentally.

IX. CONCLUSION

In this work, a computational model has been constructed that predicts the experimentally observed features of the XDT reaction. The model is based upon previously developed treatments of the equation of state (HOM) and reaction rate formula (DAGMAR). Some modifications to the DAGMAR formula were made to accommodate the XDT Reaction. The model distinguishes between damaged and undamaged propellant; the damaged propellant is much more sensitive to shock initiation than the undamaged propellant.

The computational model is developed to mimic the sequence of events thought to lead to the XDT reaction. When impact occurs between the propellant projectile and target, shock waves are propagated into both. As the shock wave propagates through the propellant, it decays as a result of the interaction with the lateral release wave emanating from the peripheral boundary. The release or tension wave grows in strength as it converges on axis. It also reflects as a tension wave and causes fractures and breakup of the propellant in the region near the impact face. This freshly damaged material is very sensitive. Material from the back of the projectile, which is still moving toward the target plate, impinges upon the damaged propellant and causes a second pressure pulse, the recompression pulse. This second pressure pulse initiates a rapid reaction in the damaged, highly sensitive propellant, and this reaction quickly builds to a detonation. This sequence of events is thought to describe the XDT process and is simulated by the computational model.

For computational convenience, most of the calculations were performed with the propellant impacting a rigid target; however, the experiments were conducted with steel target plates. A few calculations were performed with steel targets in order to determine if the loading conditions on the propellant were significantly different. Figure 19 shows results from a calculation of a 700-m/s impact between a propellant shotgun projectile and a steel plate. A comparison between Fig. 19 and Fig. 11 shows that propellant impact against a steel target and against a rigid target are very similar. The only noticeable difference between the two calculations appears to be that the XDT reaction initiates about

2 μs sooner with impact against the steel target. This comparison justifies the use of calculations involving rigid targets.

The proposed XDT model requires a pressure pulse of only about 0.1 GPa to initiate a reaction that may transform to a detonation in the damaged propellant. Therefore, a few tests were performed to determine the minimum pressure required to cause a detonation in damaged VRP propellant. These tests are described in Appendix C. It was determined that a pressure pulse with a peak pressure of only 0.12 GPa and a loading duration of only 7 μs was sufficient to cause a detonation in damaged propellant (density ratio of 85%). This magnitude impulse is consistent with the impulse available during impacts at the threshold velocity for XDT. These results substantiate the validity of the proposed XDT model.

ACKNOWLEDGMENTS

Significant contributions to this work were made by Jack Jacobson in modeling and computing and by Richard Warnes in experimenting. Typing and composition were carried out with great skill and patience by Maelo Chapin.

TABLE I

IMPACT TESTS WITH VRP PROPELLANT CYLINDERS AGAINST STEEL TARGETS[a]

Propellant Size (mm) Diam	Length	L/D	SDT Threshold Velocity (m/s)	XDT Threshold Velocity (m/s)	Time to XDT (μs)	Probability of XDT %
18	19	1.06	747	472	15-45	13
25	25	1.00	726	454	15-45	40
70	76	1.09	-	305	54-366	80
152	102	0.67	318	274	50-500	100

[a]Data taken from Ref. 5.

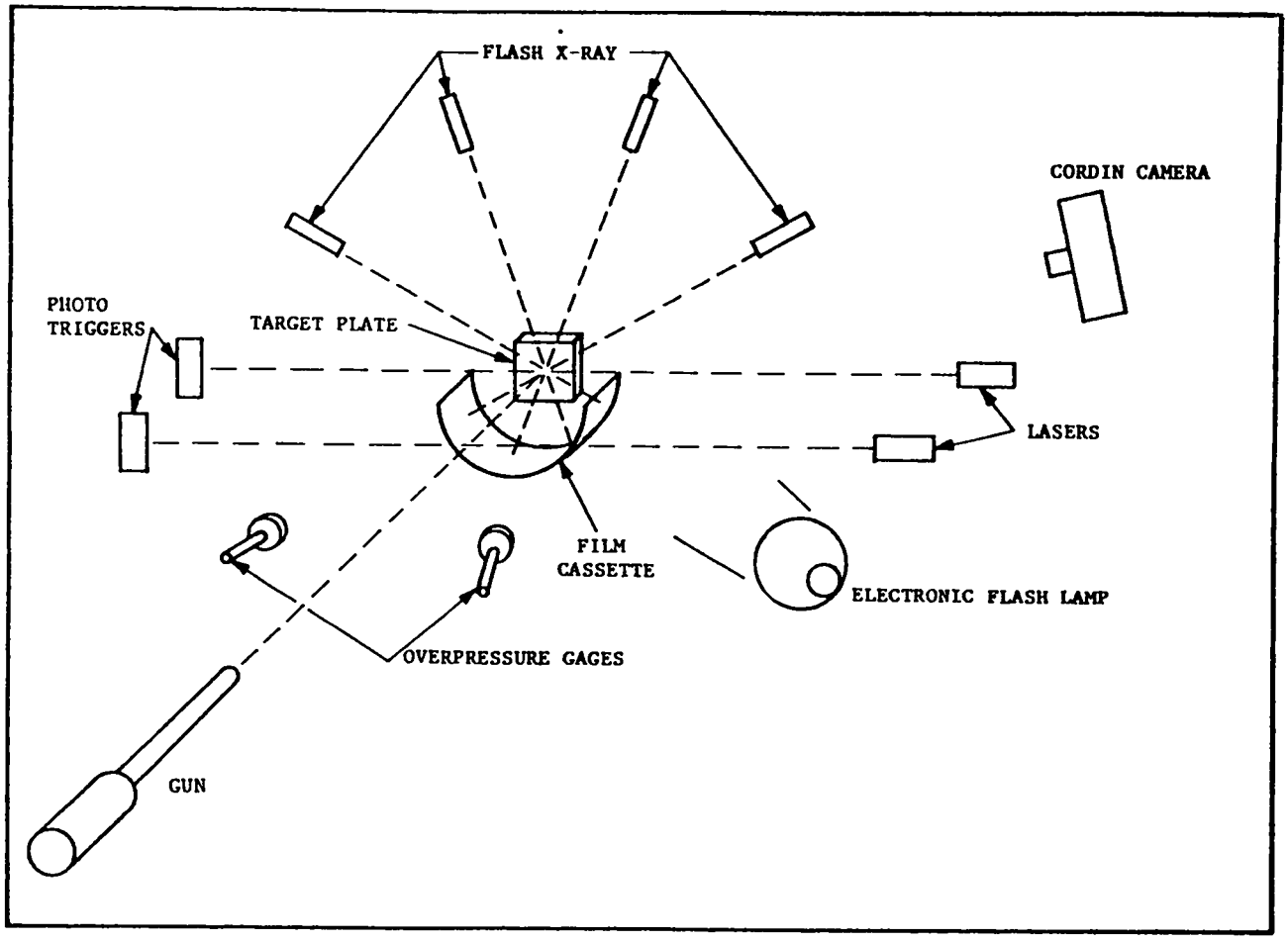

Fig. 1. Schematic of the shotgun test (from Ref. 3).

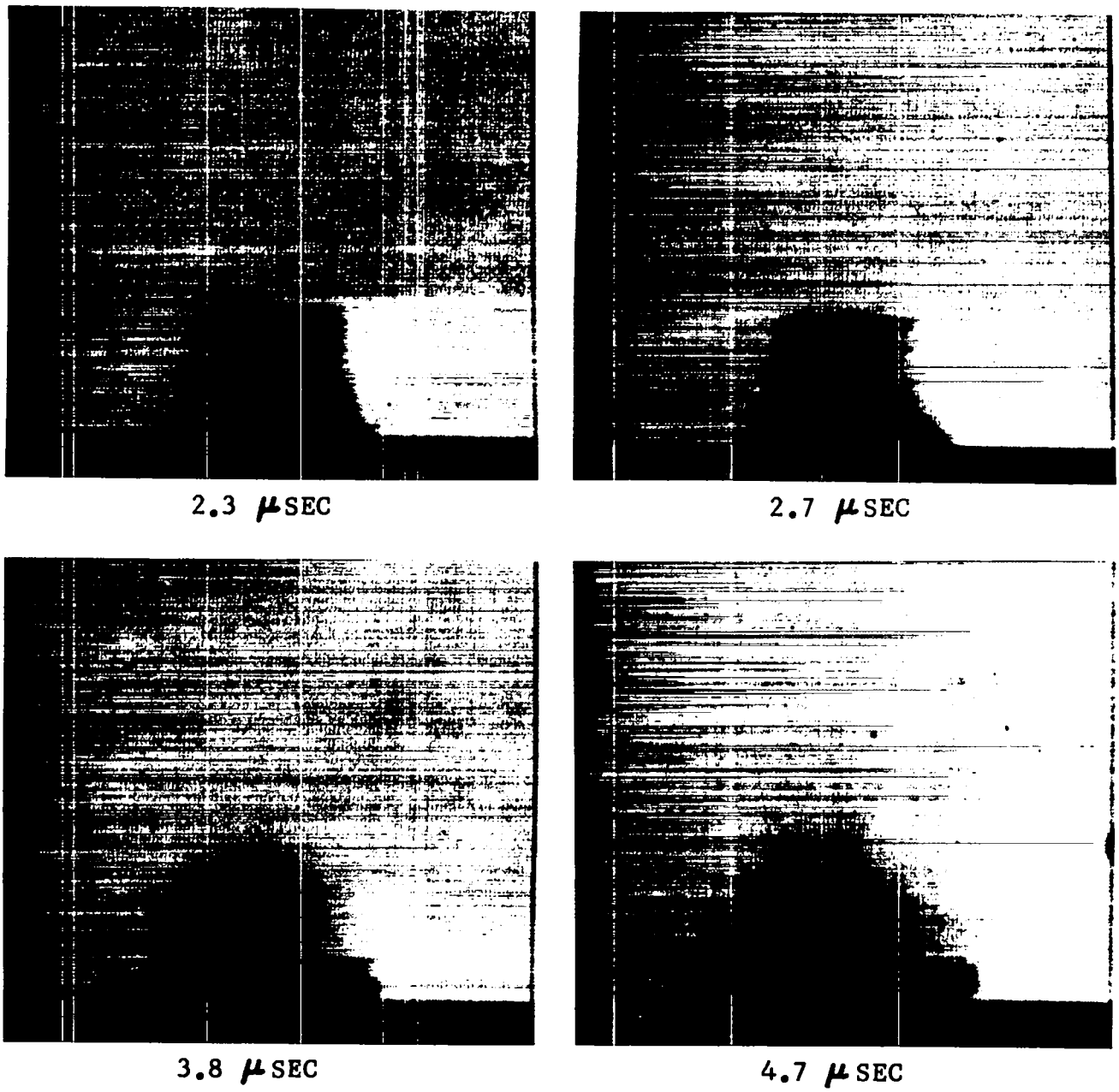

Fig. 2. Radiographs of the shotgun test showing the SDT reaction in VRP propellant (936 m/s impact velocity, from Ref. 4).

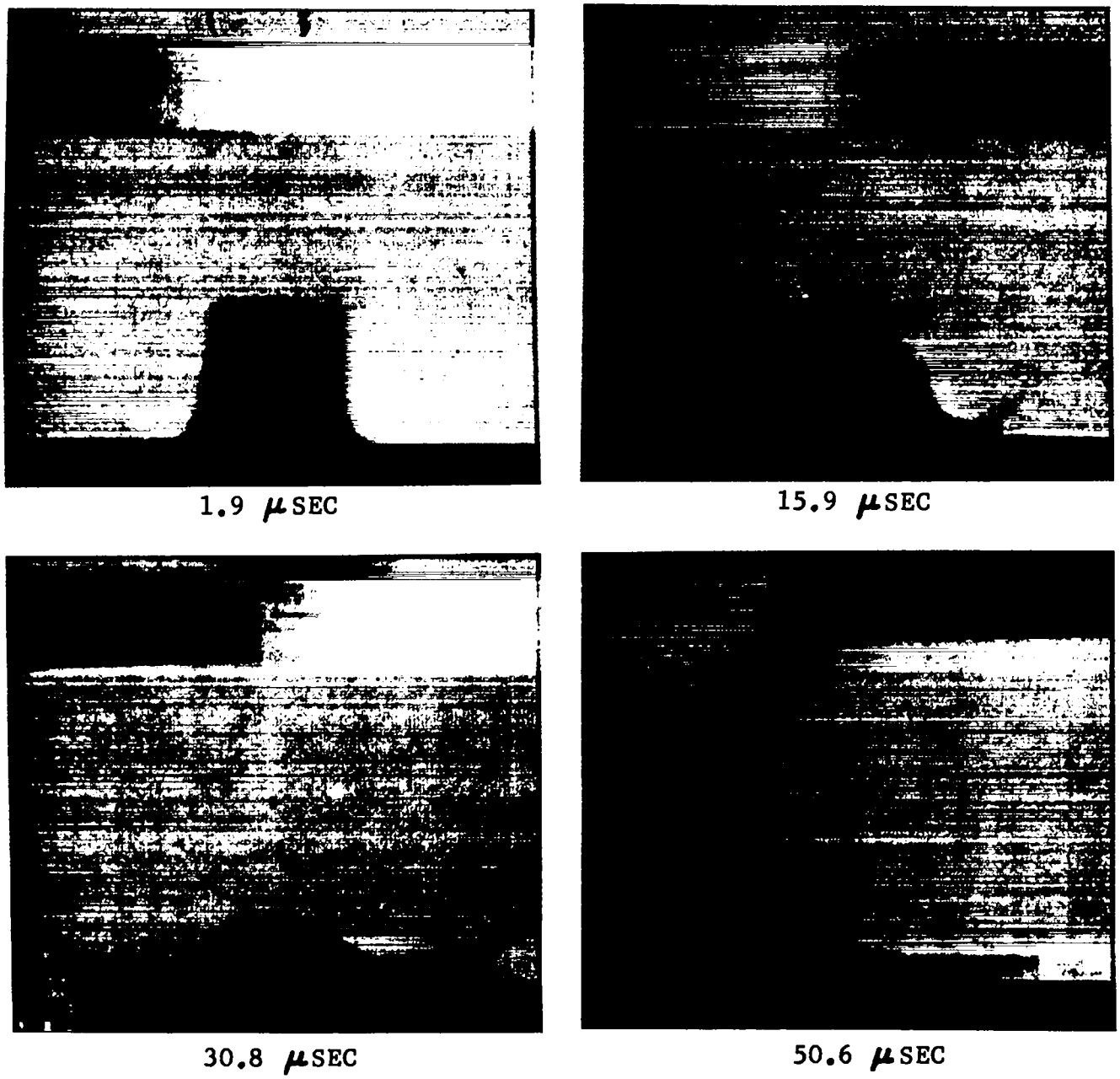

Fig. 3. Radiographs of the shotgun test showing a low-order reaction in VRP propellant (480 m/s impact velocity, from Ref. 4).

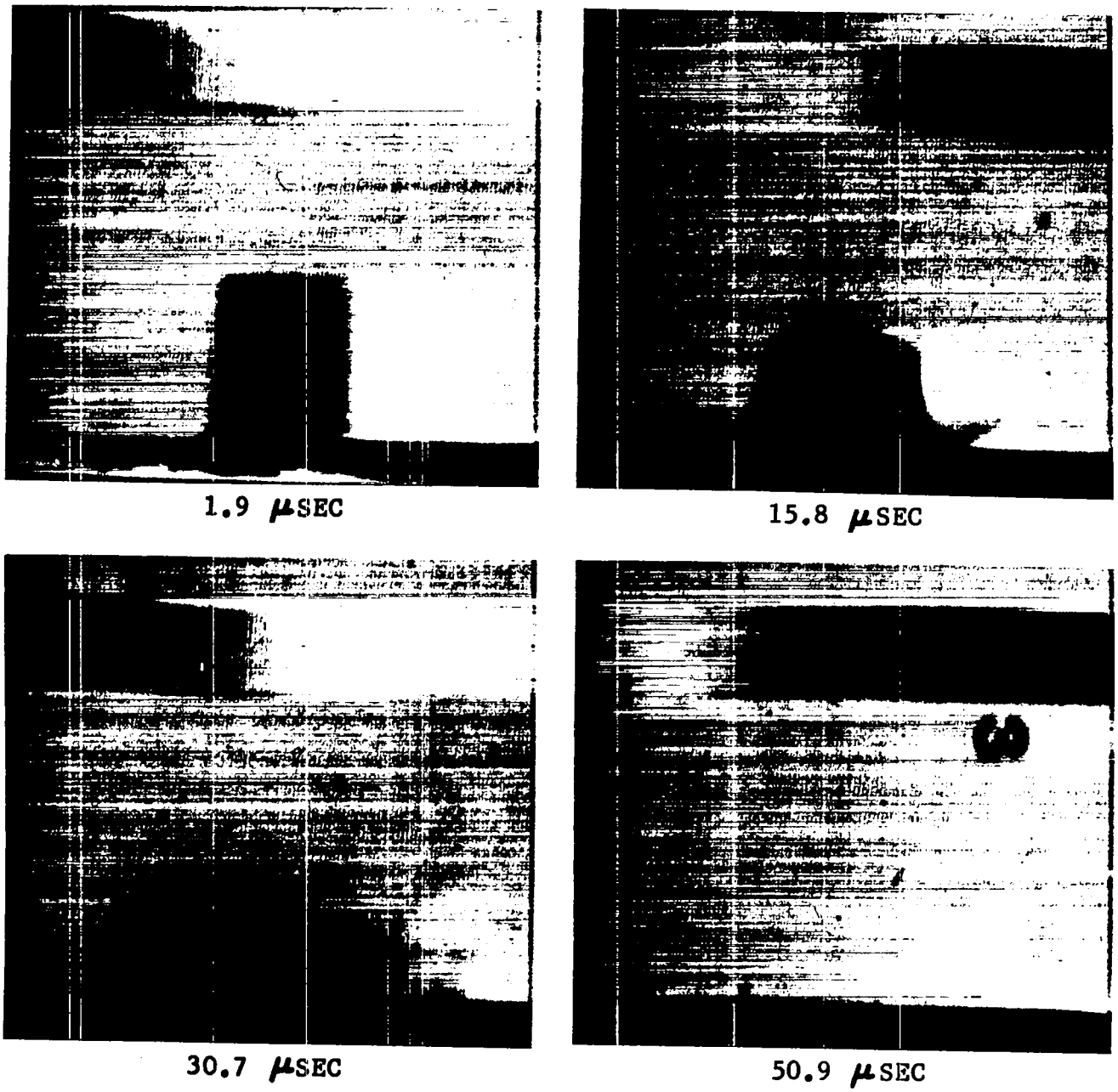

Fig. 4. Radiographs of the shotgun test showing the XDT reaction in VRP propellant (480 m/s impact velocity, from Ref. 4).

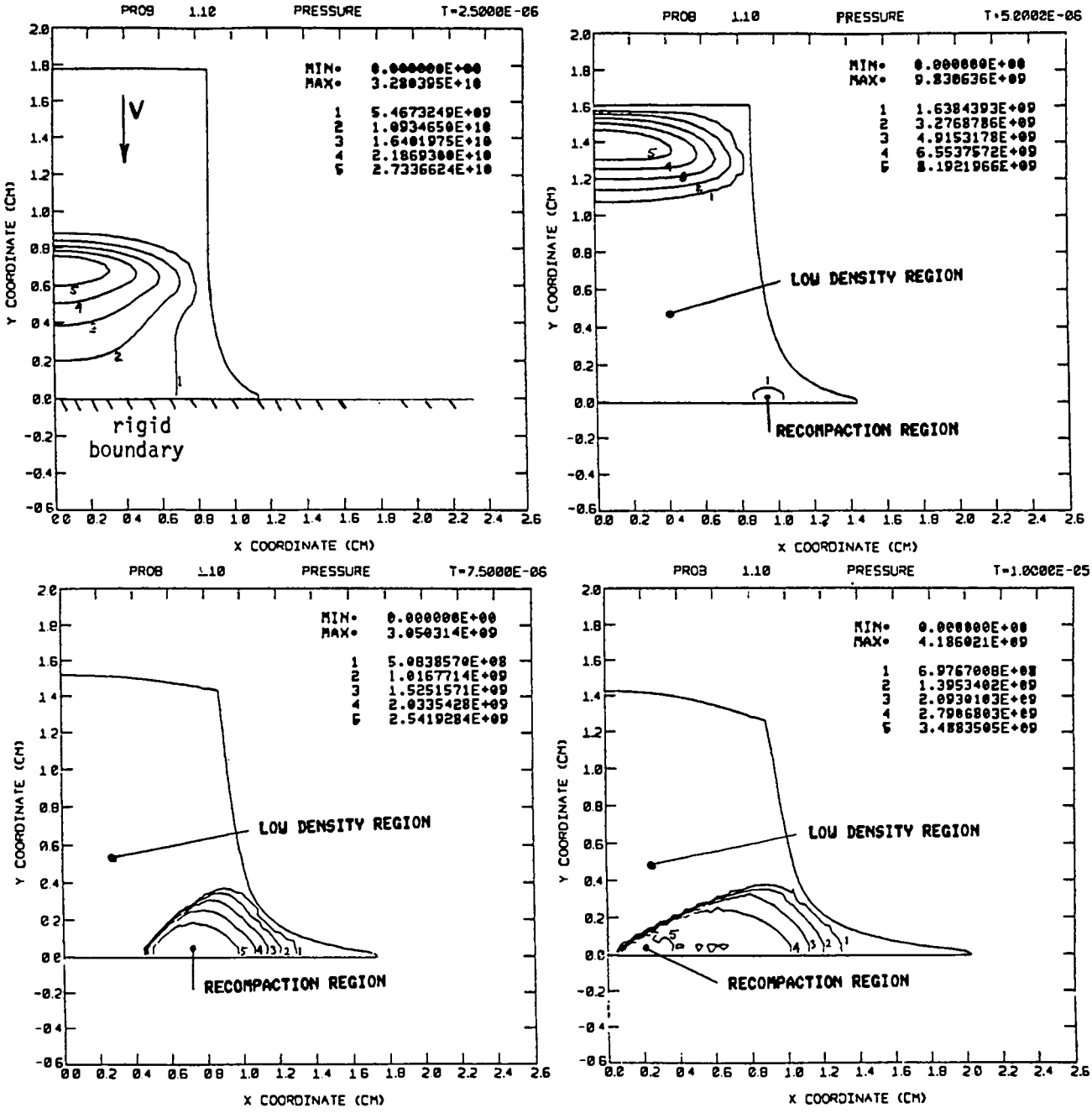

Fig. 5. Pressure contours from the calculated impact of a 700-m/s shotgun projectile of VRP propellant against a rigid target. The propellant is treated as if it were inert and without strength, and the minimum pressure allowed in the propellant is zero. The pressures listed are in dynes/cm^2. (Fig. 5 is continued on p. 19.)

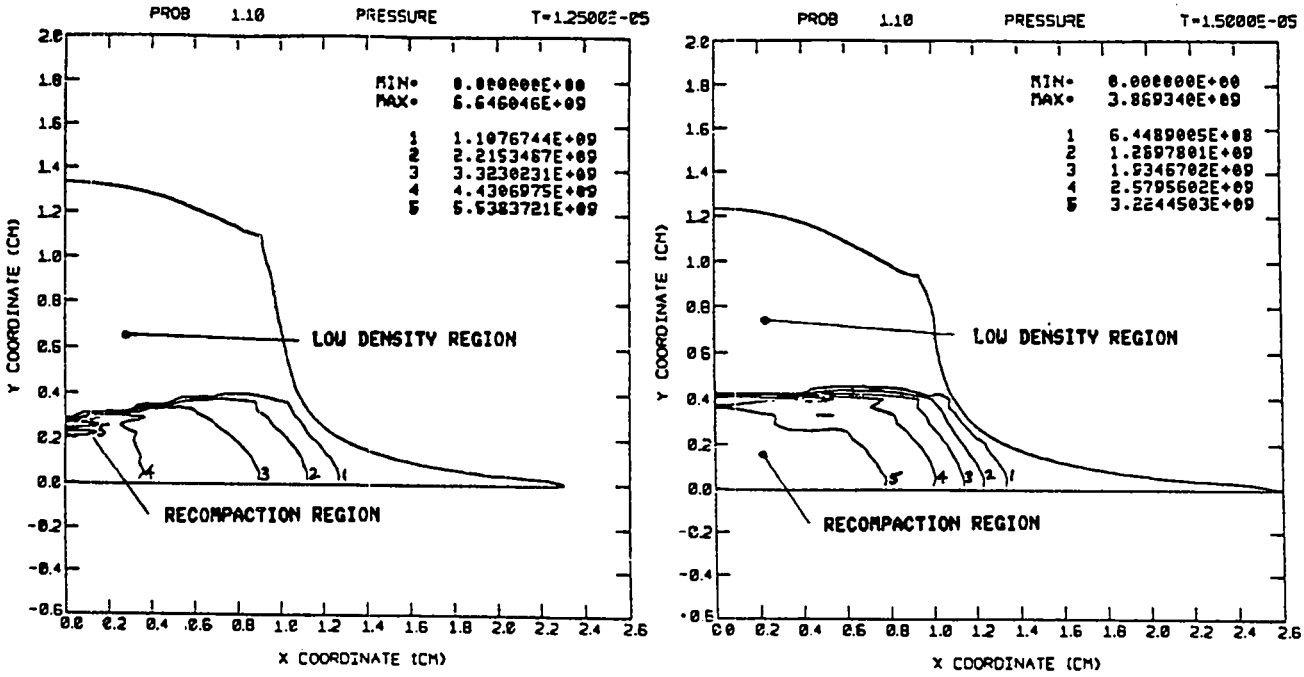

Fig. 5. (Cont'd. from p. 18.)

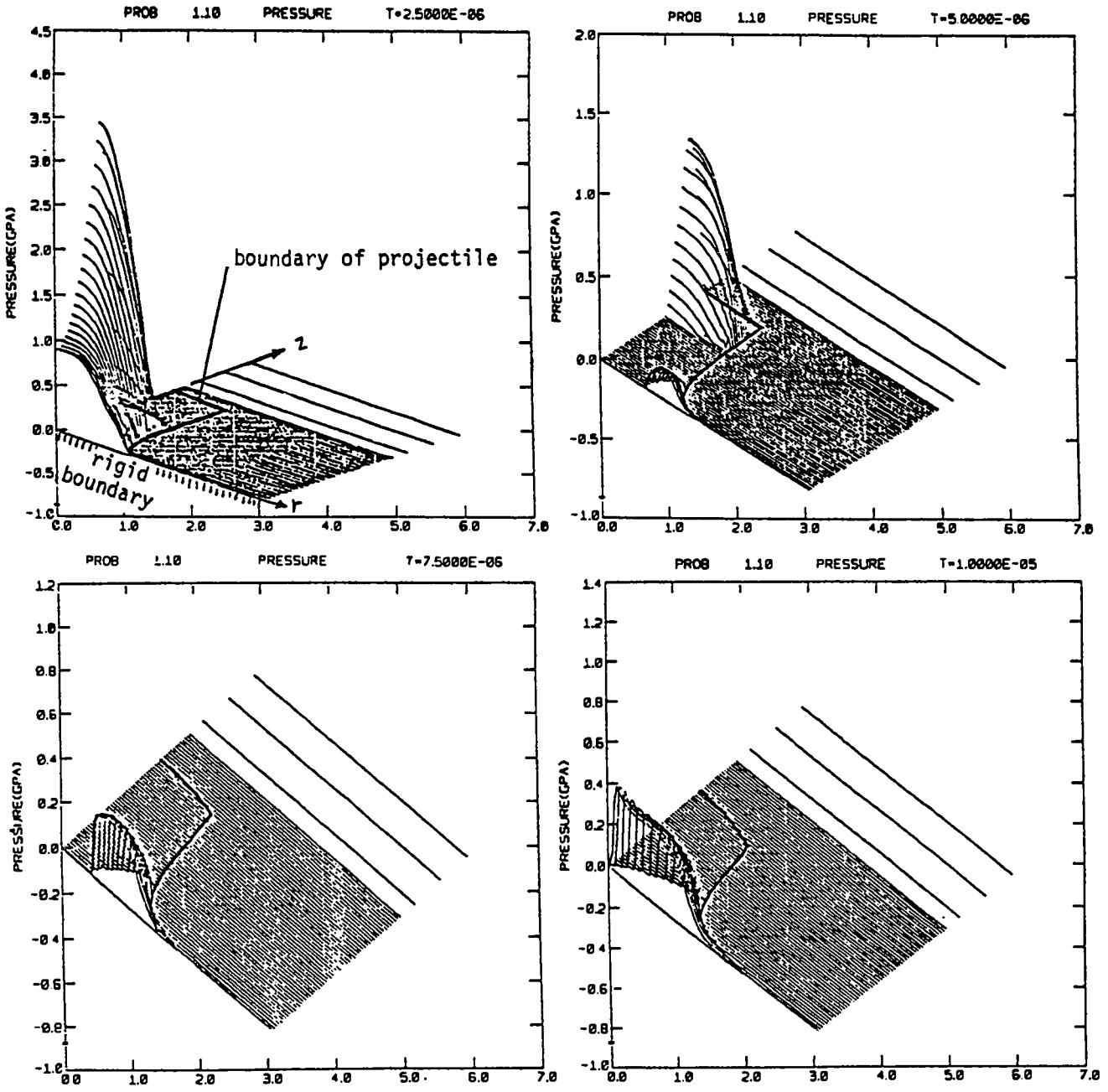

Fig. 6. The pressure distribution resulting from the calculated impact of a 700-m/s shotgun projectile of VRP propellant against a rigid target. The propellant is treated as if it were inert and without strength, and the minimum pressure allowed in the propellant is zero. Pressure is plotted vertically above the r,z plane. (Fig. 6 is continued on p. 21.)

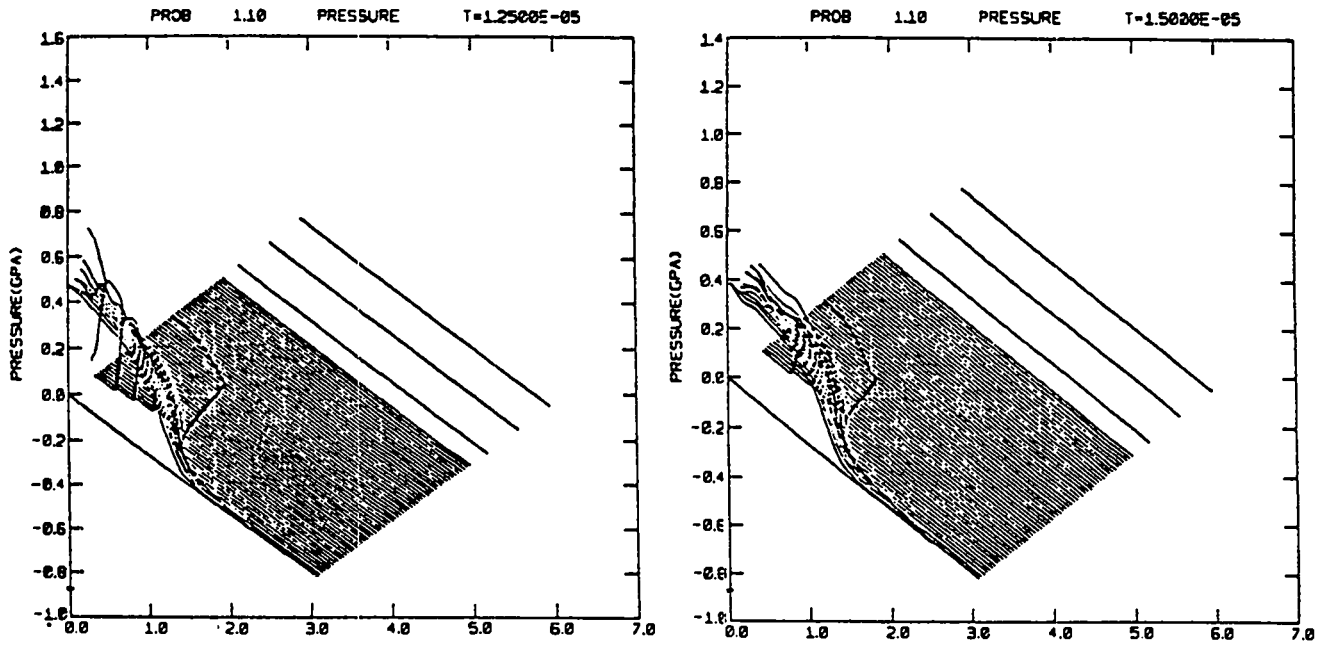

Fig. 6. (Cont'd. from p. 20.)

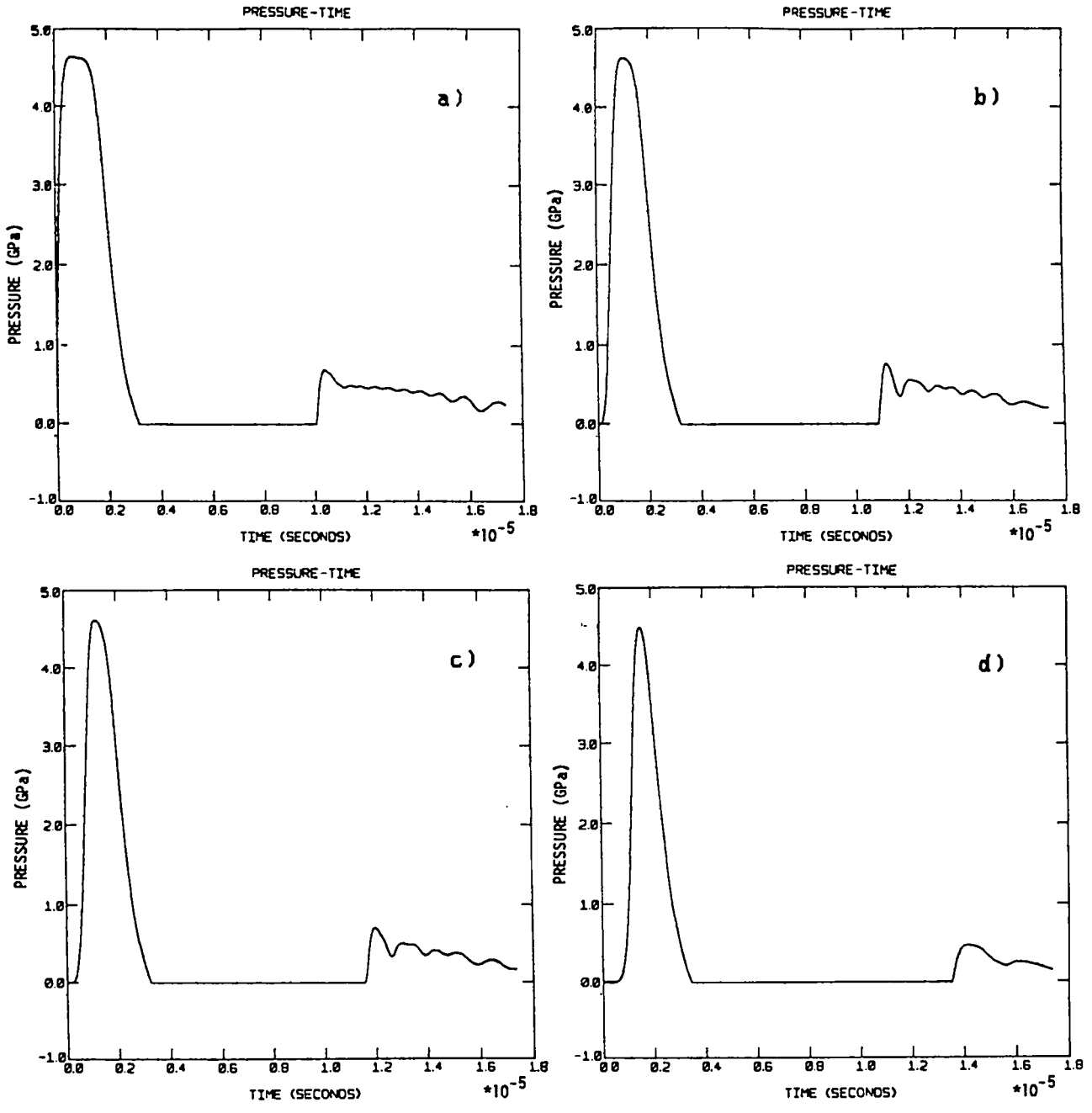

Fig. 7. The pressure history at four different points obtained from the calculated impact of a 700-m/s shotgun projectile of VRP propellant against a rigid boundary. The propellant is treated as if it were inert and without strength, and the minimum pressure allowed in the propellant is zero. The four points monitored are all near the axis of symmetry at heights of (a) 0.18 mm, (b) 1.58 mm, (c) 2.28 mm, and (d) 3.68 mm above the impact plane.

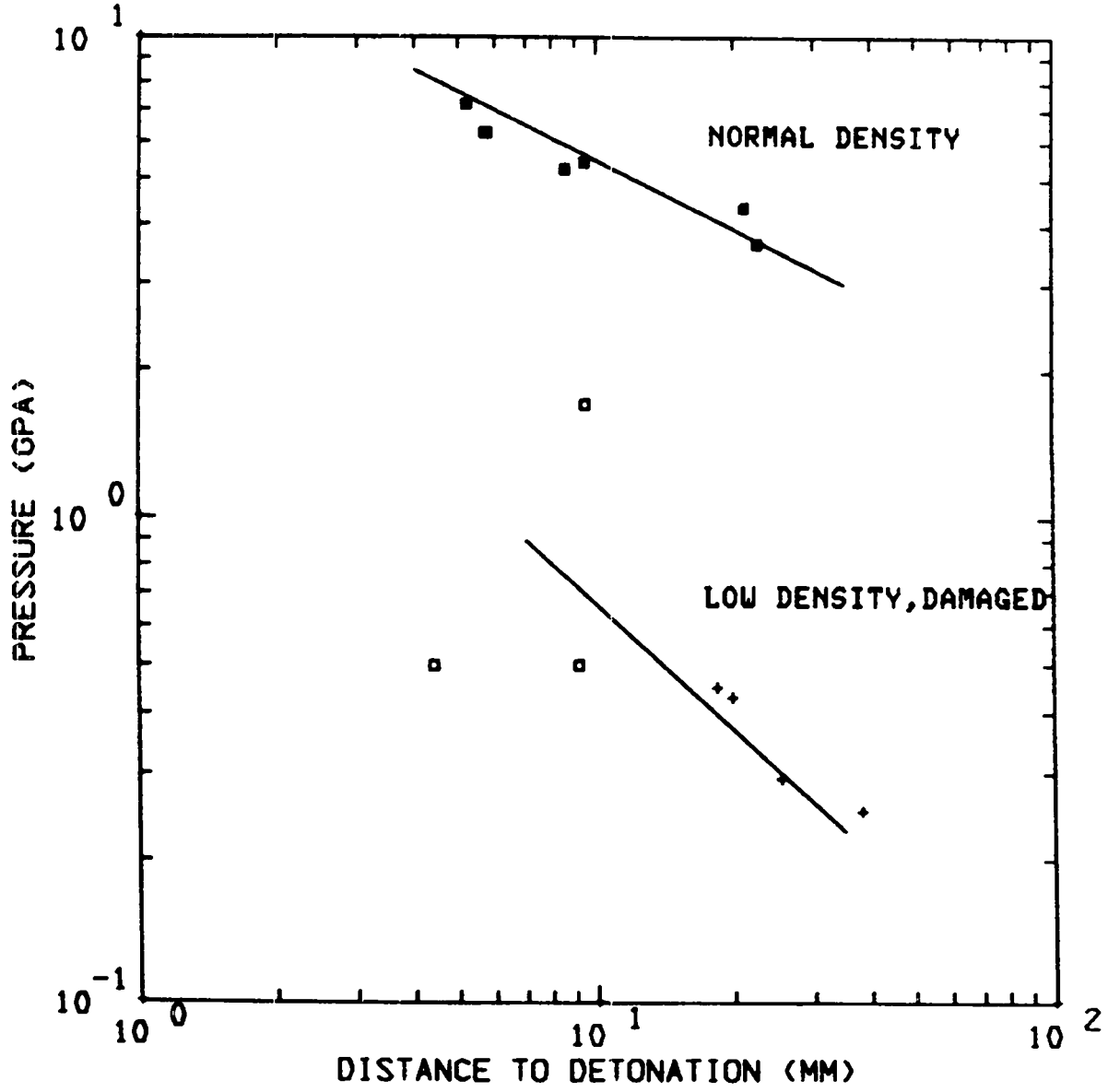

Fig. 8. The shock initiation sensitivity of some propellants represented by a plot of the input shock pressure vs run distance to detonation.

■ data points for normal-density VRP propellant (from Ref. 12)

□ data points for a low-density, damaged propellant (from Ref. 13)

\+ data points for a low-density, damaged propellant (from Ref. 14)

Upper solid line was obtained from calculations with the modified DAGMAR model for normal-density VRP propellant. Lower solid line was obtained from calculations with the modified DAGMAR model for low-density, damaged VRP propellant.

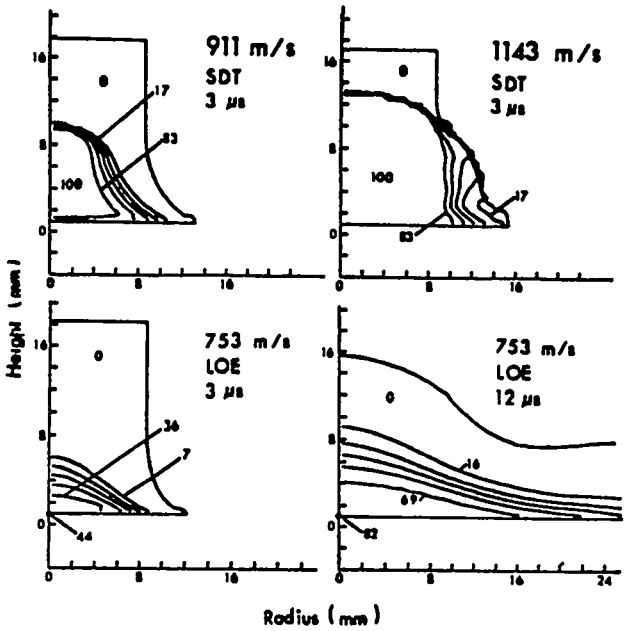

Fig. 9.

Numerical simulation of the shotgun test for three different impact speeds. Two different examples of SDT are shown in the upper frames, and one example of an impact at a speed less than the threshold speed for SDT is shown in the lower frames. The reaction model is DAGMAR for VRP propellant, and the numbers on the contours refer to the degree of reaction, λ, in per cent.

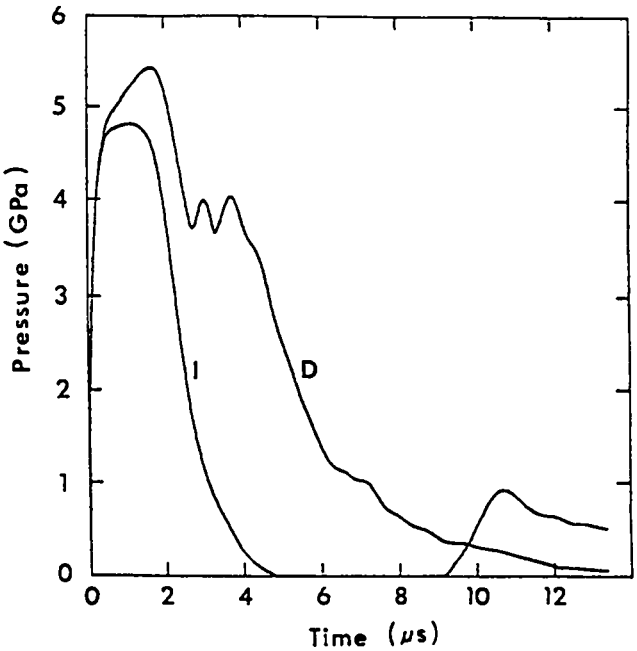

Fig. 10.

Calculated pressure histories at a point near the center of impact for the shotgun test with VRP propellant at an impact speed of 753 m/s. Curve I was obtained by modeling the propellant as an inert material. Curve D was obtained with the DAGMAR model for the propellant. The DAGMAR model predicts significant reaction that inhibits recompression.

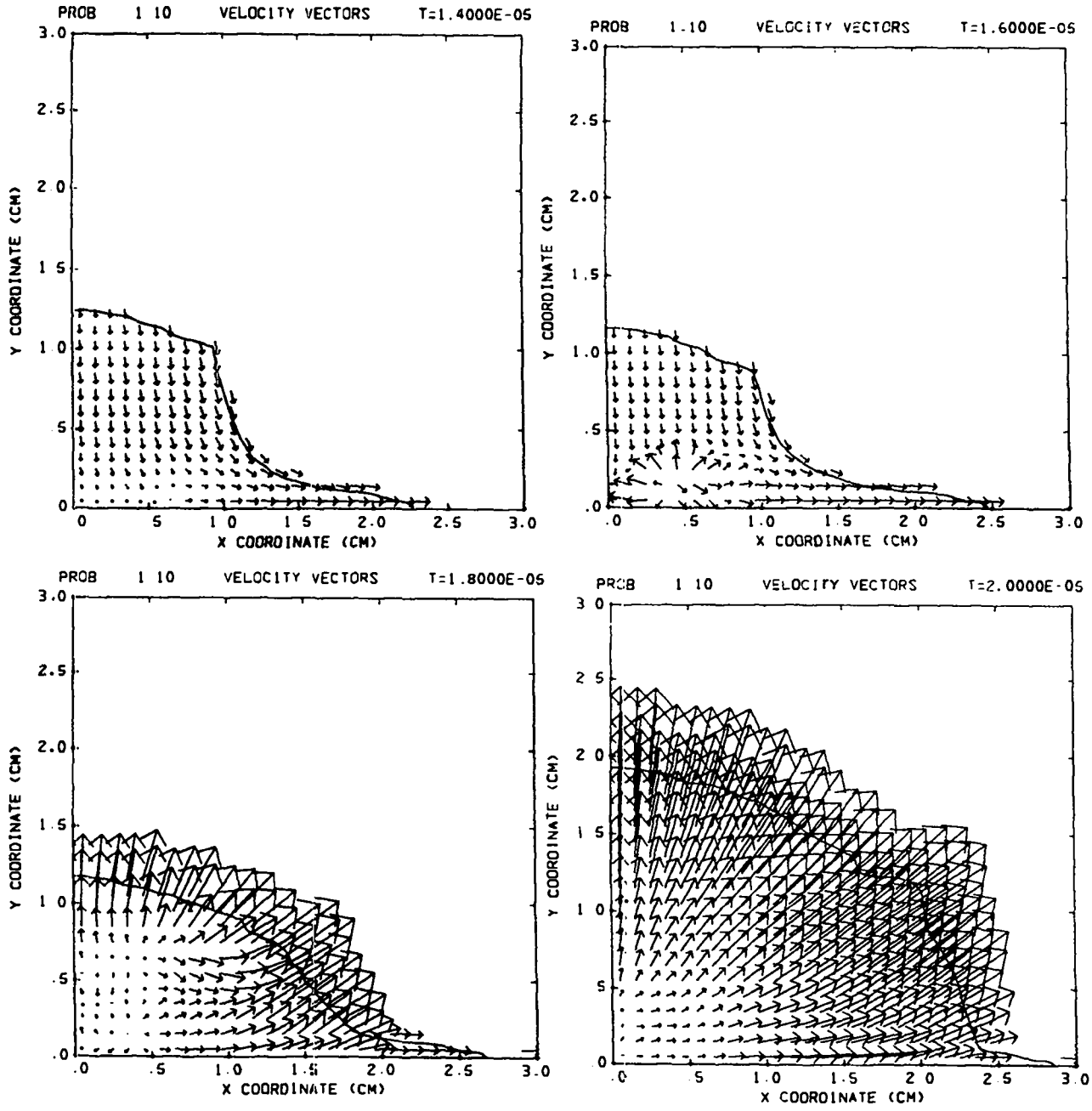

Fig. 11. Simulation of the XDT reaction. Velocity fields obtained from the calculated impact of a 700-m/s shotgun projectile of VRP propellant against a rigid target. The propellant is simulated with the modified DAGMAR model. Shear strength in the propellant is neglected, and the minimum pressure allowed in the propellant is zero. The time on each frame is in seconds.

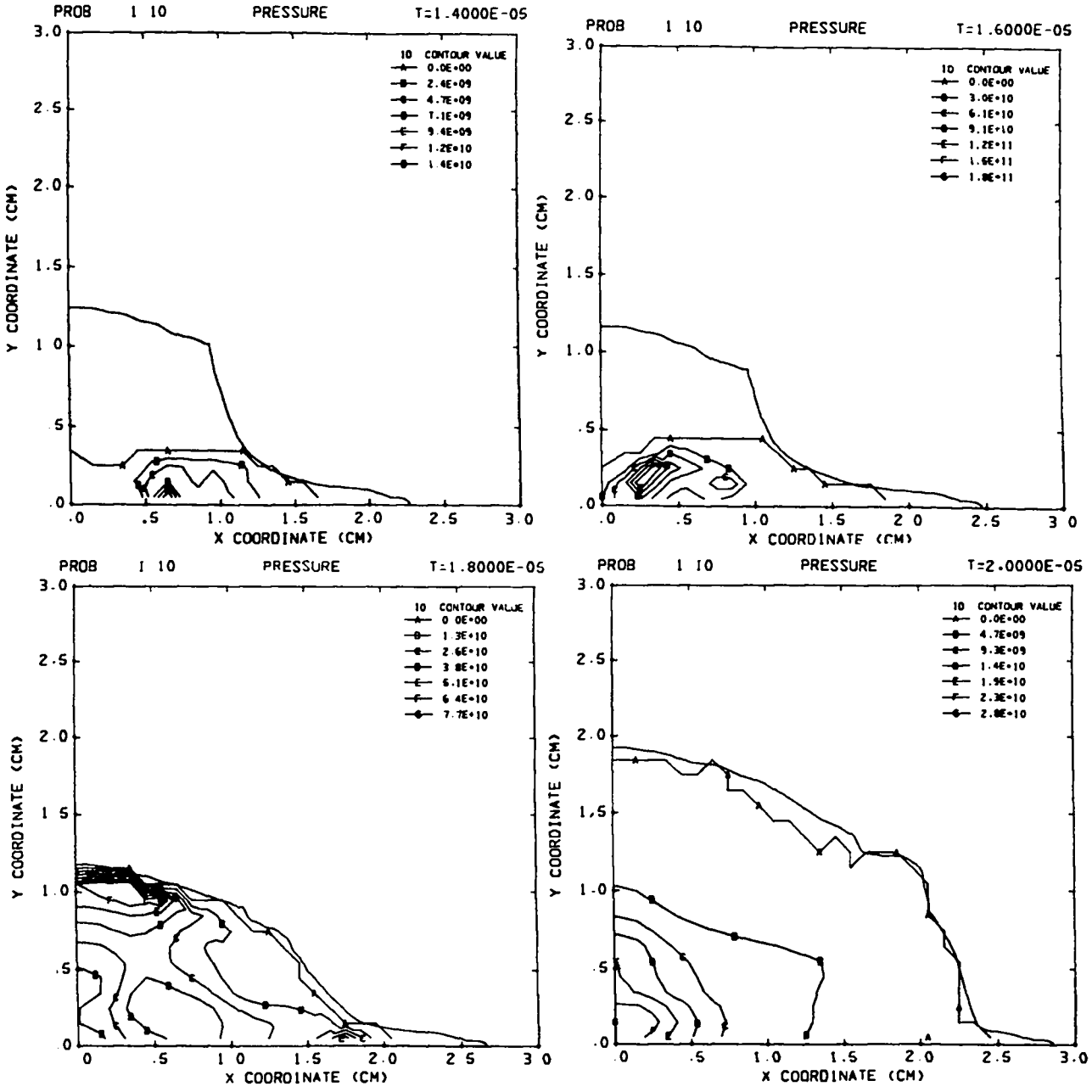

Fig. 12. Simulation of the XDT reaction. Pressure contours obtained from the calculated impact of a 700-m/s shotgun projectile of VRP propellant against a rigid target. The propellant is simulated with the modified DAGMAR model. Shear strength in the propellant is neglected, and the minimum pressure allowed in the propellant is zero. The pressures listed are in dynes/cm^2.

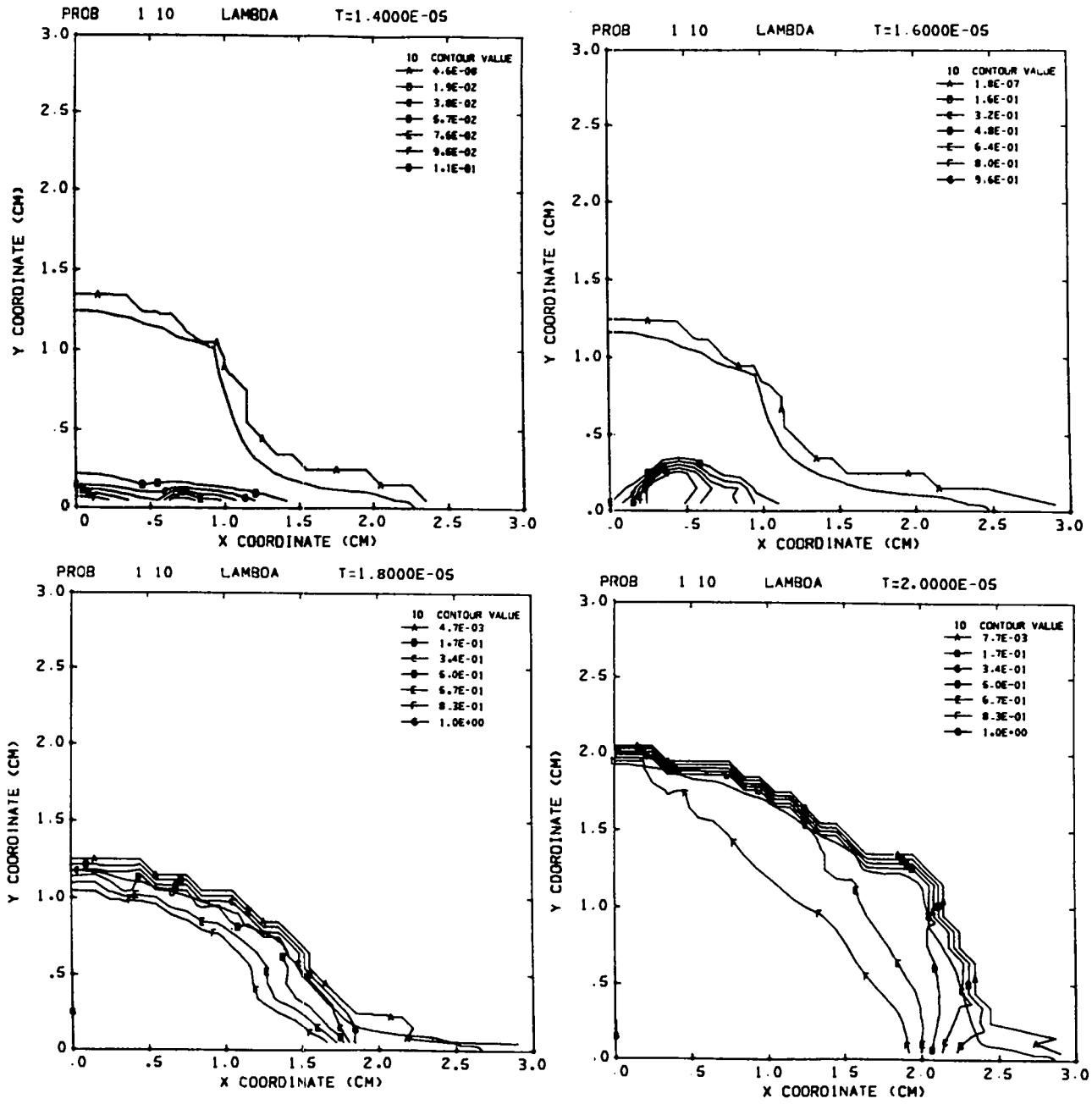

Fig. 13. Simulation of the XDT reaction. Contours of the degree of reaction obtained from the calculated impact of a 700-m/s shotgun projectile of VRP propellant against a rigid target. The propellant is simulated with the modified DAGMAR model. Shear strength in the propellant is neglected, and the minimum pressure allowed in the propellant is zero.

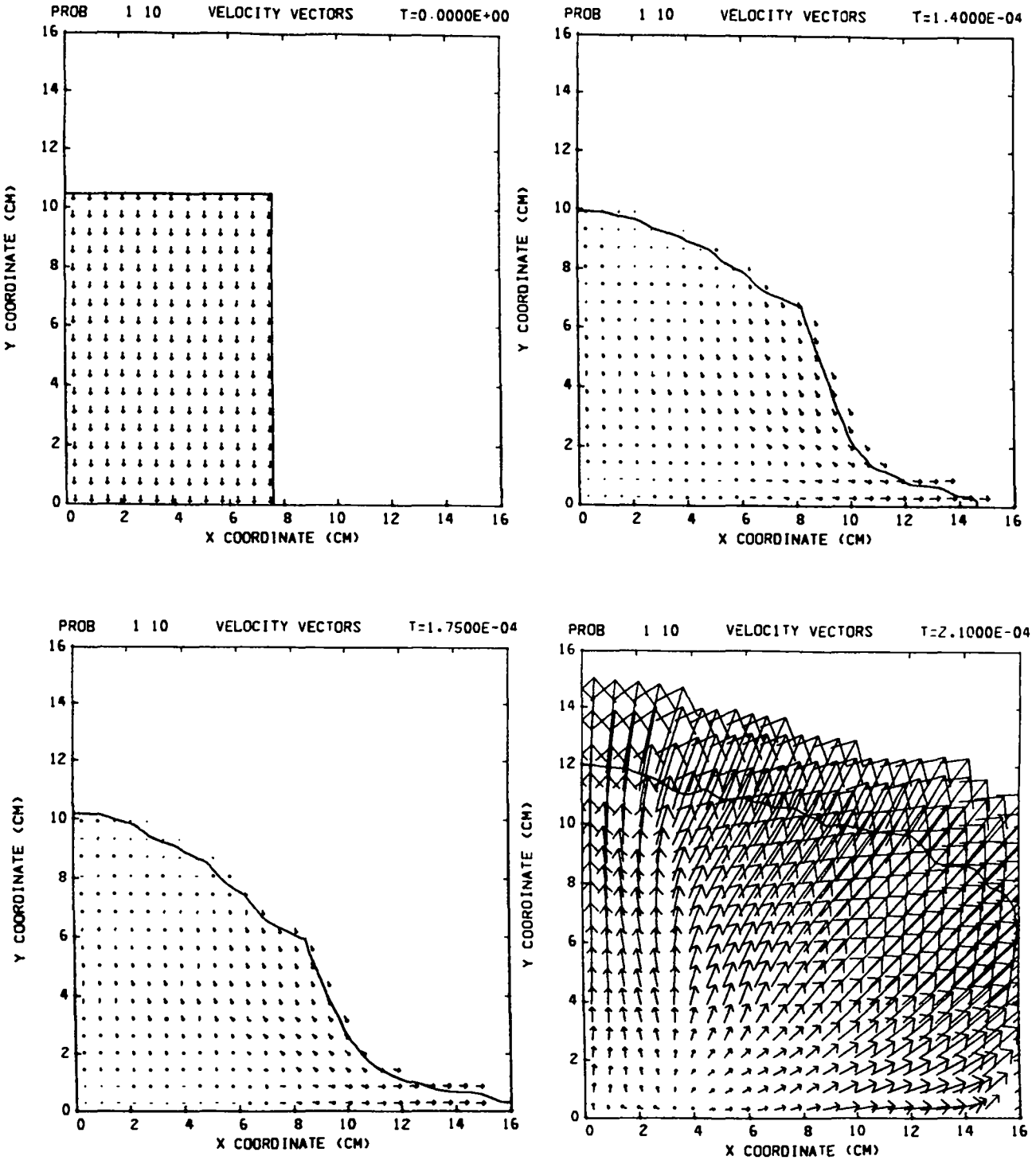

Fig. 14. Simulation of the XDT reaction. Velocity fields obtained from the calculated impact of a 152-mm-diam, 105-mm-long projectile of VRP propellant against a rigid target at 300 m/s. The propellant is simulated with the modified DAGMAR model. Shear strength in the propellant is neglected, and the minimum pressure allowed in the propellant is zero. The time on each frame is in seconds.

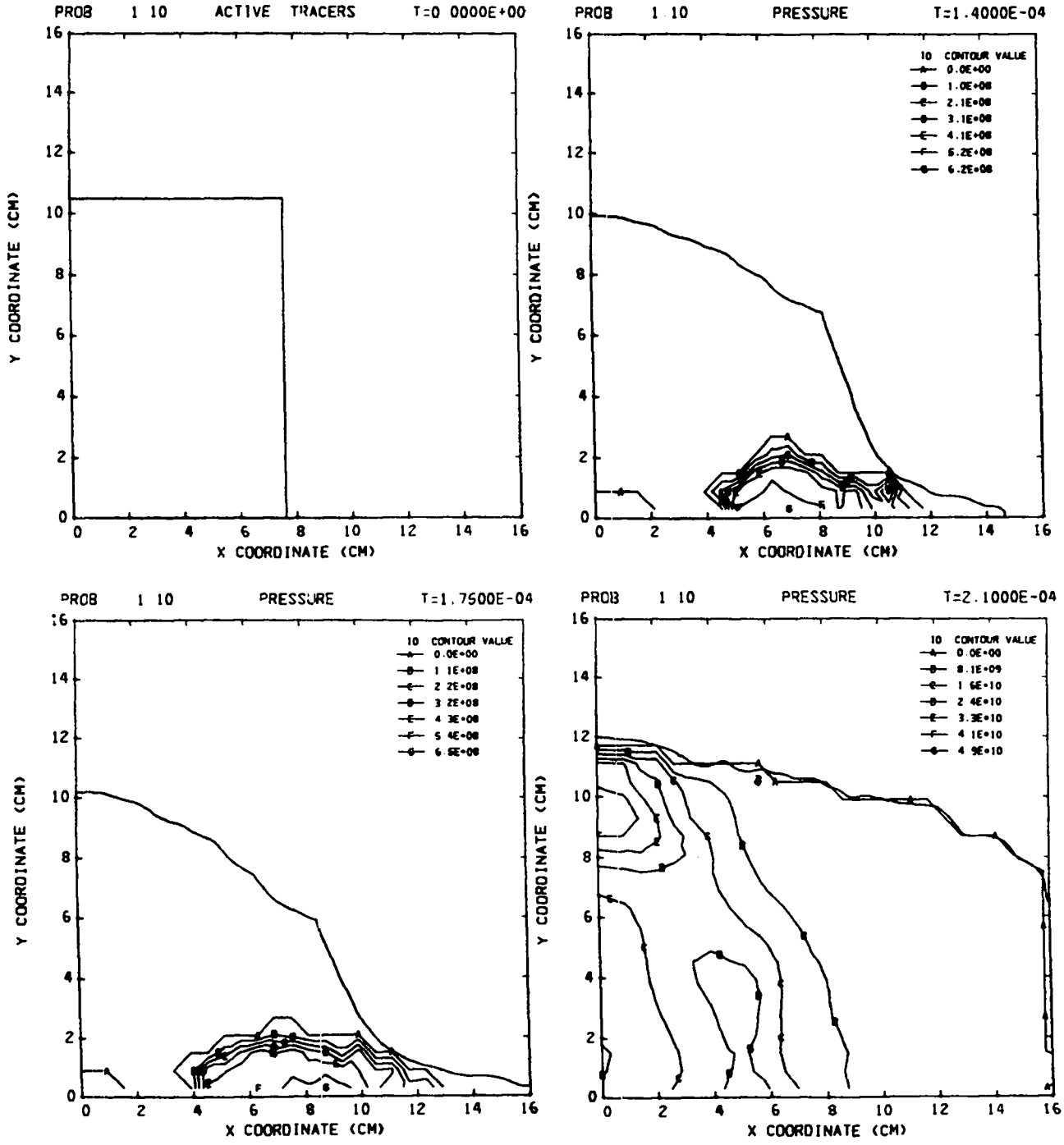

Fig. 15. Simulation of the XDT reaction. Pressure contours obtained from the calculated impact of a 152-mm-diam, 105-mm-long projectile of VRP propellant against a rigid target at 300 m/s. The propellant is simulated with the modified DAGMAR model. Shear strength in the propellant is neglected, and the minimum pressure allowed in the propellant is zero. Contour values of pressure are in dynes/cm^2.

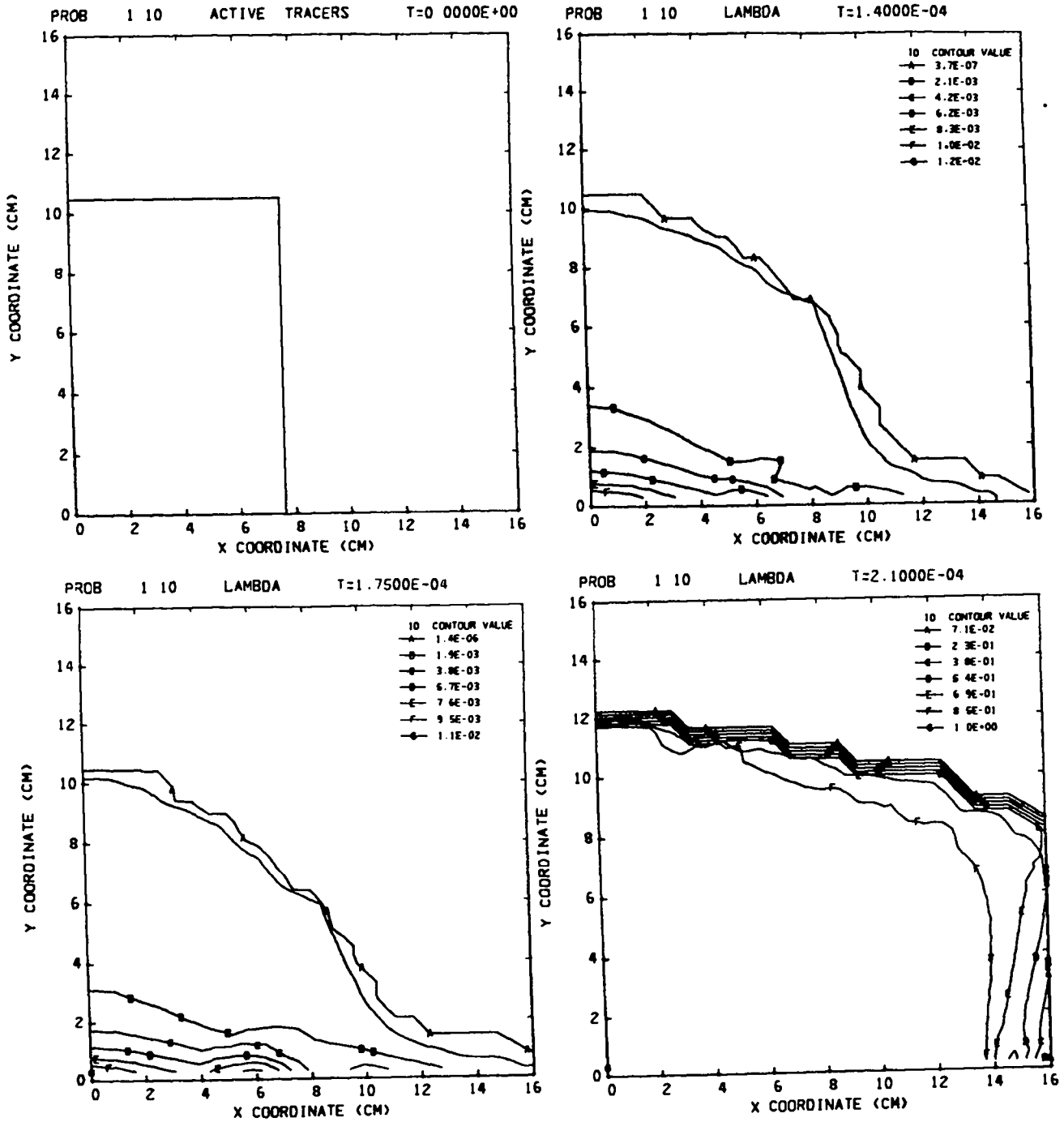

Fig. 16. Simulation of the XDT reaction. Contours of the degree of reaction obtained from the calculated impact of a 152-mm-diam, 105-mm-long projectile of VRP propellant against a rigid target at 300 m/s. The propellant is simulated with the modified DAGMAR model. Shear strength in the propellant is neglected, and the minimum pressure allowed in the propellant is zero.

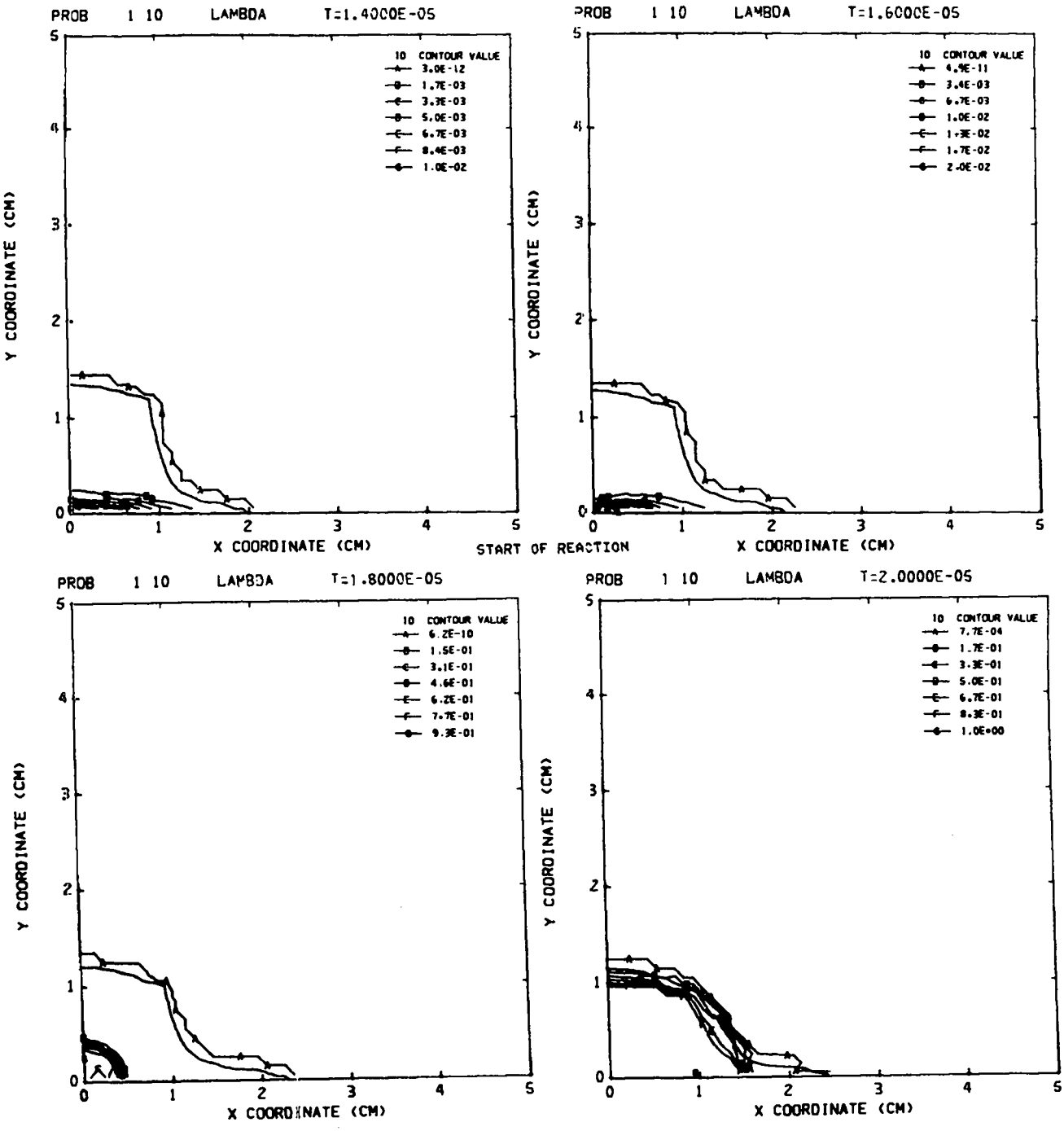

Fig. 17. Simulation of the XDT reaction. Contours of the degree of reaction obtained from the calculated impact of a shotgun projectile of VRP propellant impacting a rigid target at a low speed of 550 m/s, a speed just above the threshold velocity for XDT. At this speed, the initiation point is near the axis of symmetry (compare with Fig. 13).

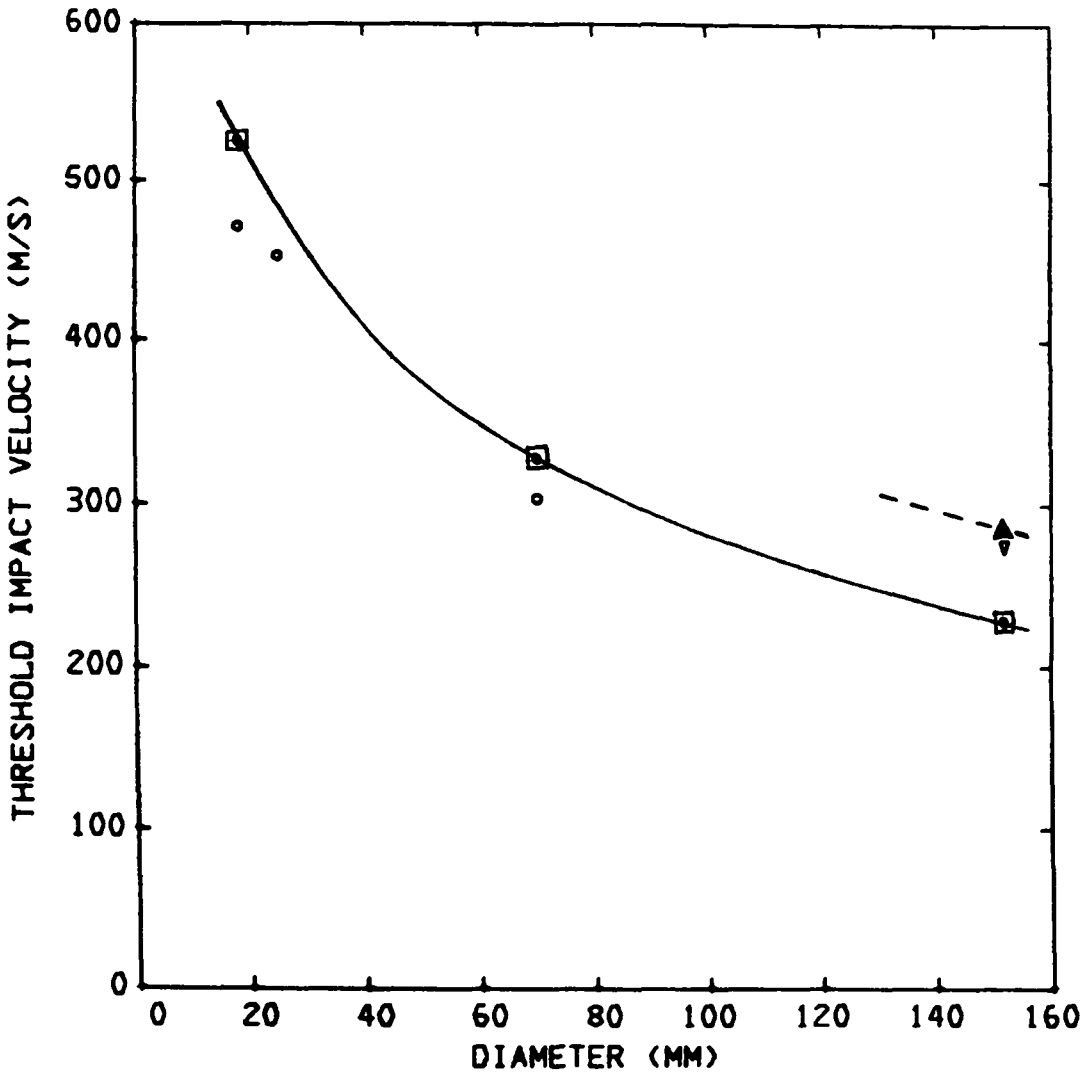

Fig. 18. Minimum impact velocity required for the XDT reaction in VRP propellant as a function of the diameter of the impacting cylindrical projectile.

⊡——⊡ Calculated threshold velocity for projectiles with L/D = 1.1

---△--- Calculated threshold velocity for a projectile with L/D = 0.7

o Experimentally determined threshold velocity for projectiles with L/D = 1.1

▽ Experimentally determined threshold velocity for projectile with L/D = 0.7

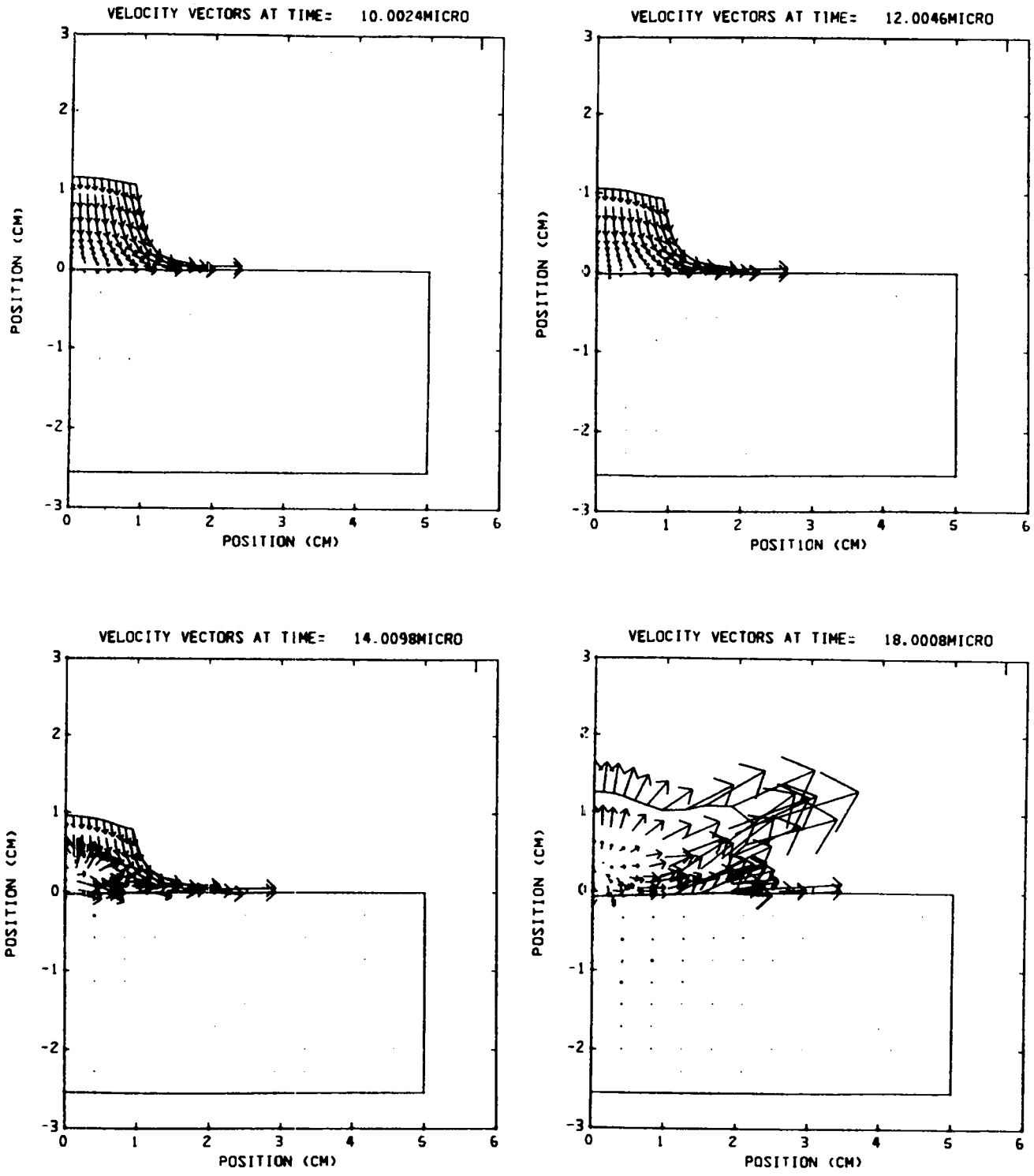

Fig. 19. Simulation of the XDT reaction. Velocity fields obtained from the calculated impact of a 700-m/s shotgun projectile of VRP propellant against a steel target. The propellant is simulated with the modified DAGMAR model. Shear strength in the propellant is neglected, and the minimum pressure allowed in the propellant is zero. The time indicated on each frame is in seconds.

APPENDIX A
THE HOM EQUATION OF STATE FOR VRP PROPELLANT

The constants used in the HOM equation of state have been determined by Bowman, Kershner, and Mader[9] for the propellant VRP. The equations used to describe the unreacted solid propellant are

$$U = c + su \quad ,$$

$$P_h = c^2(V_o - V)/[V_o - s(V_o - V)]^2 \quad ,$$

$$I_h = 1/2\ P_h(V_o - V) \quad ,$$

$$\ln T_h = \sum_{m=0}^{4} A_m(\ln V)^m \quad ,$$

$$P_S = (\Gamma/V)(I - I_h) + P_h \quad ,$$

$$T_S = (I - I_h)/C_v + T_h \quad ,$$

where U represents the shock wave speed, u the particle speed, P the pressure, V the specific volume, I the specific internal energy, and T the absolute temperature. The subscript "h" refers to quantities on the Hugoniot curve, and subscript "S" refers to the unreacted solid. The constants in the above equations, which were taken from Bowman et al., are given in the following list:

$c = 0.199$ cm/μs,

$s = 2$,

$V_o = 0.54466$ cm^3/g,

$\Gamma = 1.5$,

$C_v = 1.257 \times 10^7$ ergs/g K,

$A_o = -5.40502394255$,

$A_1 = -48.6025889997,$

$A_2 = -75.4072015339,$

$A_3 = -45.6992180220,$ and

$A_4 = -6.62503957745$ (T_h in K for V_o in cm^3/g).

The equations for the completely reacted propellant gas are

$$\ln P_i = \sum_{m=0}^{4} B_m (\ln V)^m \quad ,$$

$$\ln I_i = \sum_{m=0}^{4} C_m (\ln P_i)^m - Z \quad ,$$

$$\ln T_i = \sum_{m=0}^{4} D_m (\ln V)^m \quad ,$$

$$-1/\beta = \sum_{m=0}^{3} E_m (\ln V)^m \quad ,$$

$$P_G = (I - I_i)/(\beta V) + P_i \quad ,$$

$$T_G = (I - I_i)/C_v' + T_i \quad .$$

From Ref. 9, the constants to be used in the above equations for VRP propellant are given in the following list:

$B_0 = -3.5638038822$ $B_1 = -2.3043514451$ $B_2 = 0.3180972597$
$B_3 = -0.0394574701$ $B_4 = 0.0018643798$

$C_0 = -1.5712411395$ $C_1 = 0.5351365202$ $C_2 = 0.0767136707$
$C_3 = 0.0057634210$ $C_4 = 0.0001603569$

$D_0 = 7.9634048571$ $D_1 = -0.4822267003$ $D_2 = 0.1207672972$
$D_3 = -0.0170230990$ $D_4 = 0.0008861388$

$E_0 = D_1$ $E_1 = 2D_2$ $E_2 = 3D_3$ $E_3 = 4D_4$

$C_V' = 2.093 \times 10^7$ ergs/g K

$Z = 0.1$.

The units of the above constants are such that the specific internal energy will be given in units of Mbar $\cdot$ cm^3/g, the pressure will be given in units of Mbar, and the temperature in degrees K.

APPENDIX B
CONSTANTS FOR THE MODIFIED DAGMAR MODEL FOR VRP PROPELLANT

For the propellant in its original form, the constants to be used in Eq. (1) are

$$Z_o = 0.0075 \ (\mu s \ GPa^n)^{-1} \ ,$$

$$n = 2.75 \ ,$$

$$C_1 = 0.75 \ (GPa)^2 \ \mu s \ ,$$

$$C_2 = 0.1 \ GPa \ ,$$

$$T^* = 1200 \ K \ ,$$

$$P_I = 0.1 \ GPa \ .$$

For the propellant in a damaged state (minimum density has reached less than 95% of the original density while $\lambda < 5\%$), the constants are

$$Z_o = 0.35 \ (\mu s \ GPa^n)^{-1} \ ,$$

$$n = 1.5$$

$$C_1 = 0.75 \ (GPa)^2 \ \mu s \ ,$$

$$C_2 = 0.1 \ GPa \ ,$$

$$T^* = 1200 \ K \ ,$$

$$P_I = 0.01 \ GPa \ .$$

APPENDIX C
THE INSTRUMENTED CARD GAP TEST WITH DAMAGED VRP PROPELLANT

The purpose of this test is to estimate the sensitivity of damaged VRP propellant to an applied pressure pulse. From this test, we want to determine the ease of initiating a detonation in low density (85-90% of normal density), damaged VRP. Because recompression of damaged propellant may be the dominant ignition mechanism in the XDT reaction, we want to determine if pressures, which are consistent with pressures achieved during the recompression process of impact tests, are sufficient to cause prompt reactions in the damaged VRP. Figure C-1 shows the calculated pressure history obtained from a simulation of the 70-mm impact tests with VRP striking a steel target. The impact velocity is 305 m/s, which is equal to the threshold velocity for the XDT reaction. The peak calculated pressure occurring during recompression is about 0.15 GPa. Although pressure fluctuations exist, a substantial pressure is maintained for a considerable time. In the shotgun test, the peak recompression pressure at the threshold velocity is about twice this value, but the duration of loading is much shorter.

The test configuration, which is intended to be similar to the NOL card gap test, is illustrated in Fig. C-2. The steel confinement tube is filled with lathe shavings of VRP, which are packed to a bulk density of 85-89% of normal density. This density range is consistent with the calculated density of material to be recompressed. The Plexiglas attenuator has a diameter smaller than the tube inside diameter and is positioned a few millimeters into the tube. A P-22 planewave lens (56-mm-diam × 30-mm-long, Composition B and baratol explosives) is used as the stimulus. Seven Manganin gauges located at various positions are used to measure pressure. Gauges 1, 2, and 3 are positioned along the tube axis. They are packed with the VRP. These gauges are used to measure the input pressure pulse. The remaining gauges are mounted in a shallow grove along the inside of the steel tube and covered with a steel shim. These gauges are armored to survive the initial pressure pulse and are supposed to indicate the high pressures resulting from an eventual reaction in the propellant.

Six tests were conducted. The test configuration and results are shown in Table C-I. Tests 1 and 2 were preliminary, and no pressure gauge records were obtained. The fragmented witness plates indicated that detonations were produced. Test 3, with a 127-mm attenuator, did not produce a detonation or

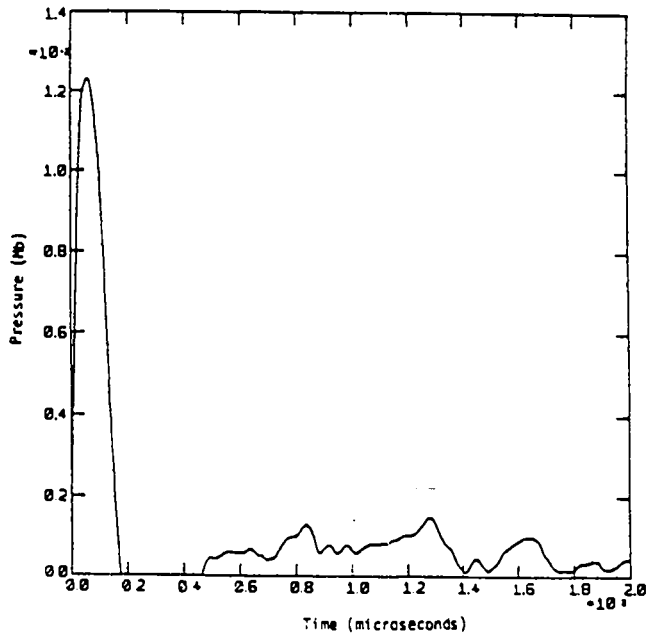

Fig. C-1. Calculated pressure history near the impact face on the axis of symmetry for the 70-mm impact test at an impact velocity of 305 m/s (threshold velocity for XDT).

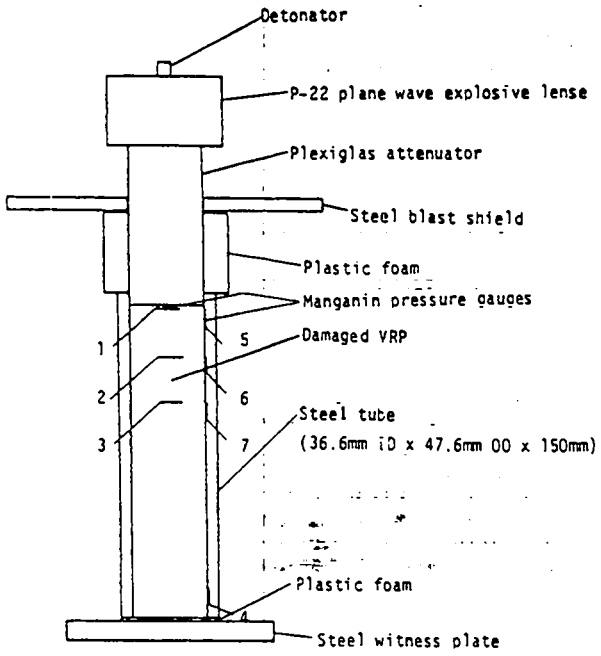

Fig. C-2. Schematic of the instrumented card gap test.

TABLE C-I

INSTRUMENTED CARD GAP TEST

Test No.	Attenuator Length (mm)	(in.)	Density Ratio Damaged / Undamaged %	Peak Pressure to Propellant (GPa)	Detonation	Time Until Detonation (μs)[a]
1	76.2	(3.0)	86	---	yes	---
2	76.2	(3.0)	86	---	yes	---
3	127.0	(5.0)	89	0.09	no	---
4	101.6	(4.0)	85	0.12	yes	30.
5	101.6	(4.0)	86	0.14	yes	43.
6	63.5	(2.5)	89	0.75	yes	13.

[a]Time between the arrival of the initial pressure pulse at gauge 1 and the recording of a high pressure by the armored pressure gauges.

significant reaction in the propellant. The applied pressure pulses were measured by gauge 1. The 0.09-GPa pressure pulse of 8-μs duration observed in Test 3 did not result in a detonation. Tests 4 and 5 were conducted with 101.6-mm attenuators, and the peak applied pressures were 0.12 and 0.14 GPa. Both tests resulted in detonations. As indicated by the armored pressure gauges, a delay of 30 and 43 μs was observed between the arrival of the input pressure pulse and occurrence of very high pressures (gauges go off scale or fail) indicating significant reaction. In Test 6, the attenuator was reduced in length to 63.5 mm in order to cause prompt initiation. This length was chosen to produce an input pressure of about 0.5 GPa. However, the gauge record shows an initial pressure of 0.75 GPa followed by a continuous rise to 2.2 GPa. This initial high pressure is probably due to reaction. From the records of gauges 6 and 7, the full detonation appears to have occurred somewhere between these gauges (about 25 mm from the attenuator). The detonation velocity measured between gauges 7 and 4 was 7.3 mm/μs.

In summary, these results indicate the damaged VRP propellant is extremely sensitive to shock initiation. A pressure pulse of just over 0.1 GPa acting for only 7 μs can initiate a detonation in 85% dense, damaged VRP propellant. This magnitude of stimulus is available in the pressure pulse associated with recompression in the shotgun, 25-mm, and 70-mm impact tests. However, there is a considerable delay between the arrival of the incident pressure pulse and detection of a violent reaction. Therefore, the smaller sized impact tests would not be expected to detonate because there is not enough material present for confinement and buildup. At a higher pressure (0.75 GPa), an almost immediate reaction occurs, which builds to a detonation in 13 μs. A 0.75-GPa shock in undamaged propellant causes no reaction. Even at this pressure loading, which is typical for recompression in the shotgun test, the run distance to detonation is longer than the remaining projectile length. However, all the incident pressure pulses used in these tests were of short duration. Response of the damaged VRP may be more immediate to a sustained pulse. These propellants were damaged long before testing. It would be interesting to see if freshly damaged propellant is even more sensitive. Also, it would be helpful to know the effect of fragment size, shape, and porosity on sensitivity.

REFERENCES

1. L. J. Hageman, D. E. Wilkins, R. T. Sedgwick, and J. L. Waddell, "HELP: A Multi-material Eulerian Program for Compressible Fluid and Elastic-Plastic Flows in Two Space Dimensions and Time," Systems, Science and Software report SSS-R-75-2654 (July 1975).

2. A. A. Amsden, H. M. Ruppel, and C. W. Hirt, "SALE: A Simplified ALE Computer Program for Fluid Flow at All Speeds," Los Alamos Scientific Laboratory report LA-8095 (June 1980).

3. "Trident-I (C-4) Motor Detonation Assessment Report," prepared by Hercules-Thiokol for Lockheed Missiles and Space Company, Inc., Sunnyvale, California, January 2, 1979.

4. "Trident-I (C- 4) Motor Behavior Studies Report," prepared by Hercules-Thiokol for Lockheed Missiles and Space Company, Inc., Sunnyvale, California, January 31, 1979.

5. "Trident-I (C-4) Detonation Modeling Support Study, Final Report," prepared by Hercules-Thiokol for Lockheed Missiles and Space Company, Sunnyvale, California, October 1982.

6. E. Fugelso, J. D. Jacobson, R. R. Karpp, and R. Jensen. "Radiographic Study of Impact in Polymer-Bonded Explosives," in Shock Waves in Condensed Matter - 1981, Eds. W. J. Nellis, L. Seaman, and R. A. Graham, AIP Conference Proceedings No. 78.

7. Charles L. Mader, Numerical Modeling of Detonation, University of California Press, Berkeley and Los Angeles, California, 1979, p. 324.

8. L. G. Green, E. James, E. L. Lee, E. S. Chambers, C. M. Tarver, C. Westmoreland, A. M. Weston, and B. Brown, "Delayed Detonations in Propellants from Low Velocity Impact" in the Seventh Symposium (International) on Detonation, U S Naval Academy, Annapolis, Maryland, June 16-19, 1981.

9. A. L. Bowman, J. D. Kershner, and C. L. Mader, "Numerical Modeling of Sympathetic Detonation," Los Alamos Scientific Laboratory report LA-7989 (November 1979).

10. J. Wackerle, R. L. Rabie, M. J. Ginsberg, and A. B. Anderson, "A Shock Initiation Study of PBX-9404," in The Symposium on High Dynamic Pressure, Paris, France, August 28-30, 1978.

11. W. Fickett, "PAD, A One-Dimensional Lagrangian Hydrocode," Los Alamos National Laboratory report LA-5910-MS (April 1975).

12. J. J. Dick and J. B. Ramsay, "Shock Sensitivity and Hugoniots of VTG-5a and VRP Propellants," Los Alamos National Laboratory internal report M-3-78-U-5 (May 3, 1978).

13. J. R. Travis, "Shock Initiation of Granulated VOY-7 Propellants," Los Alamos National Laboratory internal report M-3-QR-79-3 (March 1979).

14. "Trident-I (C-4) Detonation Modeling Support Study Progress Report," prepared by Hercules-Thiokol for Lockheed Missiles and Space Co., Inc., Sunnyvale, California, May 21, 1982.

☆U.S. GOVERNMENT PRINTING OFFICE: 1984—577-034/4220